

ARTICLE

Activation of group 2 innate lymphoid cells alleviates aging-associated cognitive decline

Ivan Ting Hin Fung¹, Poornima Sankar¹, Yuanyue Zhang¹, Lisa S. Robison², Xiuli Zhao³, Shanti S. D'Souza¹, Abigail E. Salinero², Yue Wang³, Jiang Qian⁴, Marcy L. Kuentzel⁵, Sridar V. Chittur⁵, Sally Temple³, Kristen L. Zuloaga², and Qi Yang^{1,6}

Increasing evidence has challenged the traditional view about the immune privilege of the brain, but the precise roles of immune cells in regulating brain physiology and function remain poorly understood. Here, we report that tissue-resident group 2 innate lymphoid cells (ILC2) accumulate in the choroid plexus of aged brains. ILC2 in the aged brain are long-lived, are relatively resistant to cellular senescence and exhaustion, and are capable of switching between cell cycle dormancy and proliferation. They are functionally quiescent at homeostasis but can be activated by IL-33 to produce large amounts of type 2 cytokines and other effector molecules in vitro and in vivo. Intracerebroventricular transfer of activated ILC2 revitalized the aged brain and enhanced the cognitive function of aged mice. Administration of IL-5, a major ILC2 product, was sufficient to repress aging-associated neuroinflammation and alleviate aging-associated cognitive decline. Targeting ILC2 in the aged brain may provide new avenues to combat aging-associated neurodegenerative disorders.

Introduction

The brain has been traditionally viewed as an immune-privileged organ largely devoid of immune cells save for microglia in the parenchyma (Carson et al., 2006). Nevertheless, advances in the past decade have instead suggested a critical role for immune surveillance in maintaining the physiological function of the brain (Louveau et al., 2015; McGowan et al., 2011; Wolf et al., 2009). RAG-deficient mice lacking adaptive immune cells or mice deficient for T cells exhibited impaired neurogenesis and declined cognitive function that could be restored by the transfer of splenocytes or CD4⁺ T cells (McGowan et al., 2011; Wolf et al., 2009). Exacerbated progression of Alzheimer's disease phenotype has also been observed in *Rag2*^{-/-}*Il2rg*^{-/-} mice that lack both adaptive and innate lymphocytes (Marsh et al., 2016). The mechanisms of immune-mediated cognitive protection are not yet fully understood. Th2 T cell-derived cytokines IL-4 and IL-13 have been shown to preserve spatial learning and memory through reducing inflammation and promoting neurogenesis (Brombacher et al., 2017; Derecki et al., 2010). Regulatory T cells (T reg cells) may also alleviate cognitive decline in mouse models of Alzheimer's disease, possibly by constraining neuroinflammation (Baruch et al., 2015; Dansokho et al., 2016; Ito et al., 2019). The theory of immune surveillance is

centered on the importance of circulating adaptive immune cells, with the meninges being the major interaction site between the peripheral immune system and the brain. However, the properties of potential noncirculating tissue-resident lymphocytes in the brain remain poorly understood. The function and regulation of lymphocytes residing in more specialized structures with closer proximity to the brain parenchyma, such as the choroid plexus (CP), are also largely unexplored.

Aging is a complex process leading to progressive loss of physiological functions in multiple organs and systems (López-Otín et al., 2013). The brain is particularly susceptible to the effects of aging. Mammalian cognitive function, especially learning and memory, gradually declines with aging (Glisky, 2007; Harada et al., 2013). Whether and how immune cells may affect this process remains unknown. Aging is known to induce gradual deterioration of the adaptive immune system and to increase susceptibility to infectious diseases, termed immunosenescence (Goronzy and Weyand, 2013). However, the effects of aging on the immune system are much more complicated than a pan-decrease in immune cell development and function. Interestingly, many tissue-resident innate immune cells, such as microglia, display

¹Department of Immunology and Microbial Disease, Albany Medical College, Albany, NY; ²Department of Neuroscience and Experimental Therapeutics, Albany Medical College, Albany, NY; ³Neural Stem Cell Institute, Rensselaer, NY; ⁴Department of Pathology, Albany Medical College, Albany, NY; ⁵Center for Functional Genomics, University at Albany–State University of New York, Rensselaer, NY; ⁶Department of Medicine, Albany Medical College, Albany, NY.

Correspondence to Qi Yang: yangq@amc.edu; Kristen L. Zuloaga: zuloagk@amc.edu.

© 2020 Fung et al. This article is distributed under the terms of an Attribution–Noncommercial–Share Alike–No Mirror Sites license for the first six months after the publication date (see <http://www.rupress.org/terms/>). After six months it is available under a Creative Commons License (Attribution–Noncommercial–Share Alike 4.0 International license, as described at <https://creativecommons.org/licenses/by-nc-sa/4.0/>).

hyperactivation phenotypes with aging (Dilger and Johnson, 2008; Spittau, 2017). In addition, subsets of memory or memory-like T and B cells with innate-like properties have been observed to accumulate with aging (Fukushima et al., 2018; Goronzy and Weyand, 2017; Hao et al., 2011; Ratliff et al., 2013; Rubtsov et al., 2011; Rubtsova et al., 2015). The increased numbers and activity of certain innate or innate-like immune cell subsets with aging might be considered as host responses to compensate for the drastic decline in adaptive immune cell development and function. Such responses are generally considered detrimental, leading to increased basal levels of inflammation and susceptibility to inflammatory diseases with aging, termed inflammaging (Franceschi et al., 2018). However, it remains unknown whether aging may also possibly select unique populations of immune cells with enhanced cellular fitness and preserved beneficial capability that can instead be harnessed to combat aging.

Innate lymphoid cells (ILC) are specialized innate effectors that lack clonally distributed antigen receptors, but transcriptionally resemble T cells (Yang and Bhandoola, 2016). Group 2 ILC (ILC2) respond to the alarm protein IL-33 and are potent producers of IL-5 and IL-13 (Yang and Bhandoola, 2016). ILC2 are noncirculating, tissue-resident cells residing at nonlymphoid tissues such as mucosal barrier sites, the uterus, and adipose tissues (Yang and Bhandoola, 2016). Local proliferation, but not recruitment from the periphery, is a signature of ILC2 activation (Gasteiger et al., 2015). Tissue-resident ILC2 are implicated in tissue repair, tissue remodeling, and metabolic homeostasis (Vivier et al., 2018). ILC2 were recently discovered in the dura sinus of the meninges of young mice (Gadani et al., 2017). Meningeal-resident ILC2 are activated during spinal cord injury and are involved in healing after spinal cord injury (Gadani et al., 2017). However, whether ILC2 also reside in other specialized brain barrier structures, such as the CP, remains unknown, and their potential role in cognitive function and their responses to aging remain to be investigated.

In this study, we report the accumulation of tissue-resident ILC2 in the CP of the aged brain, with ILC2 comprising a major subset of lymphocytes in the CP of aged mice and humans. ILC2 in the aged brain are long-lived and capable of reversibly switching between cell cycle dormancy and proliferation. They are relatively resistant to cellular senescence and exhaustion under replication stress, leading to enhanced self-renewal capability. They are functionally quiescent at homeostasis but can be activated by exogenous IL-33 to produce large amounts of IL-5 and IL-13 as well as a variety of other effector molecules in vitro and in vivo. When activated in vitro and transferred intracerebroventricularly (i.c.v.), they revitalized the aged brains and enhanced cognitive function of aged mice. Administration of IL-5, a major ILC2 product, repressed aging-associated neuroinflammation and alleviated aging-associated cognitive decline. Together, these results suggest that aging may expand a unique population of brain-resident ILC2 with enhanced cellular fitness and potent neuroprotective capability. Targeting ILC2 in the aged brain may unlock therapies to combat aging-related neurodegenerative disorders.

Results

Tissue-resident ILC2 accumulate in the CP of aged brains

The CP, which produces cerebrospinal fluid and forms a specialized blood–cerebrospinal fluid barrier, may harbor a variety of circulating and tissue-resident immune cells. To investigate the effects of aging on brain neuroimmunity, we performed a genome-wide microarray analysis comparing the gene expression profiles of the CP of young (2–3 mo) versus aged (18–22 mo) C57/BL6 mice. Interestingly, we detected an upregulation of a range of ILC2 lineage characteristic genes in the CP of aged mice, leading to the hypothesis that ILC2 may accumulate in the aged brain (Fig. S1). These genes include the master transcription factors *Gata3* and *Bcl11b* that drive ILC2 development and maintain ILC2 identity; ILC2 characteristic cytokine receptors *Il7r*, *Il2ra*, *Il2rg*, and *Crlf2*; ILC2 maturation marker *Klrg1*; and ILC2 characteristic adhesion molecule *Icam1* (Fig. S1). We therefore directly examined the cellularity and phenotype of ILC2 in the brains of young and aged mice by flow cytometry. Indeed, aged mice had a three- to fivefold increase in ILC2 numbers in the brain over young mice (Fig. 1, A and B). ILC2 in aged brains were of comparable size and exhibited similar expression of key molecules, such as GATA-3, T1/ST2 (IL-33R), and IL7R, to those in young mice (Fig. 1 C). We next used an established i.v. anti-CD45.2 PE antibody labeling method to determine whether the accumulated brain ILC2 in aged mice were in circulation or were tissue resident (Anderson et al., 2014). Almost no ILC2 were labeled with i.v. injected anti-CD45.2 PE antibody, indicating that ILC2 in both young and aged brains are noncirculating, brain-resident cells (Fig. 1, D and E). Together, tissue-resident ILC2 accumulate in the aged brain.

We next examined the other ILC subsets in the aged brain. Natural killer (NK) cells were readily detectable in the brain, but their numbers remained unchanged with aging (Fig. 1 F). ILC1 were rare and were moderately increased in number with aging (Fig. 1 F). ILC3 were barely detectable in the brain of either young or aged mice. Thus, ILC2 represent the major ILC subset that accumulates in the aged brain (Fig. 1 F).

To determine the anatomical locality in which ILC2 reside, we examined their distribution in different regions of aged brains by flow cytometry. Brain parenchyma regions, including the cortex, prefrontal cortex, striatum, thalamus, hippocampus (HP), and subventricular zone, were devoid of ILC2 (Fig. 2 A). Notably, ILC2 were enriched in the CP of aged brains (Fig. 2 A). Previous studies indicated that ILC2 were also present in the dura sinus of young mice (Gadani et al., 2017). Because dura meninges were attached to the skull, they were not included in our whole brain preparation. We therefore additionally examined the effects of aging on meningeal ILC2. Meninges attached to the brain parenchyma were referred to as “leptomeninges.” Meninges attached to the skull consisted of dura meninges and some arachnoid meninges and were referred to as “dura/arachnoid meninges.” ILC2 were hardly detectable in the leptomeninges of young or aged mice (Fig. 2 A). Consistent with the previous report (Gadani et al., 2017), a relatively large amount of ILC2 was detected in the meninges attached to the skull, which consisted of dura meninges and some arachnoid meninges (Fig. 2 A). The number of dura/arachnoid meningeal ILC2 was

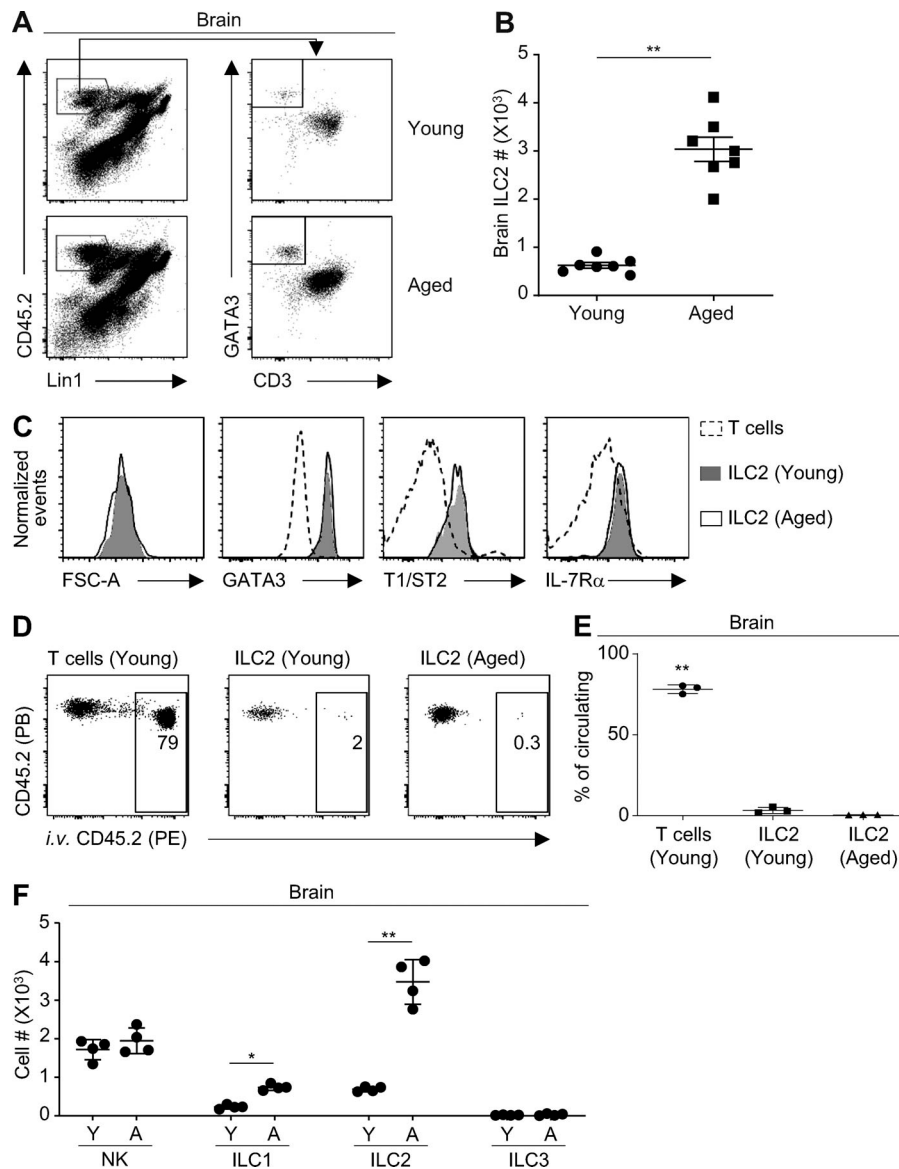


Figure 1. **ILC2 accumulate in the aged brain.** **(A)** Representative flow cytometry profiles of hematopoietic cells in the brains of young (2–3-mo-old) and aged (18–22-mo-old) mice. **(B)** Quantification of ILC2 numbers in the brains of young and aged mice. Data are from seven mice per group, pooled from two independent experiments. **(C)** Representative flow cytometry profiles of ILC2 and T cells from the brains of young and aged mice. FSC-A, forward scatter area. **(D)** Representative flow cytometry profiles of brain ILC2 and T cells from young and aged mice injected i.v. with anti-CD45.2 PE antibody and euthanized 3 min after injection. PB, pacific blue. **(E)** Percentages of circulating cells labeled with i.v. injected anti-CD45.2 PE antibody. Data are from three mice per group and are representative of two independent experiments. **(F)** The number of various ILC subsets in the brain of young (Y) and aged (A) mice. Data are from four mice per group and are representative of two independent experiments. Error bars are mean \pm SEM. *, $P < 0.05$; **, $P < 0.01$.

moderately increased with aging (Fig. 2 A). Of note, age-related increase of meningeal ILC2 was rather moderate (around only twofold), in contrast to the drastic accumulation of CP ILC2 with aging (Fig. 2 A). Indeed, ILC2 represented a major lymphocyte subset in the CP of aged mice, making up ~50% of the lymphocytes present in the CP (Fig. 2 B). The other ILC subsets, including NK cells, ILC1, and ILC3, were barely detectable in the CP of aged mice (Fig. 2 C). Strikingly, unlike the aged brain, the CP of young mice did not contain a significant amount of ILC2, indicating that the accumulation of ILC2 in the CP is a signature of aging (Fig. 2, E and F). Whole-mount immunofluorescence staining verified that ILC2 were readily detectable in the CP of aged mice but not in the CP of young mice (Fig. 2 G). The accumulation of ILC2 in the CP was gradual with age, starting as early as 6 mo of age (Fig. 2 H). Flow cytometry analysis of CP tissue from deceased elderly people revealed that ILC2 were also a major subset of lymphocytes in the CP of aged humans (Fig. 2 I). Human CP ILC2 in aged individuals expressed high amounts of CRTH2 but not c-Kit (Fig. 2 J). Human CP ILC2 also

expressed relatively high amounts of mRNA for *IL5* and *IL13* but not *IL17A* (Fig. 2 J). Together, these data demonstrate that tissue-resident ILC2 accumulate in the CP of aged brains.

ILC2 in the aged brain are long-lived and exhibit enhanced cellular fitness

To explore the mechanisms by which ILC2 accumulate in the aged brain, we examined the proliferation capability and life span of brain ILC2 in young and aged mice. Interestingly, compared with ILC2 in the brains of young mice, ILC2 from the aged brain expressed less *Mki67* mRNA (Fig. 3 A). Flow cytometry analysis verified that ILC2 from aged brains had significantly lower expression of Ki67 compared with their young counterparts, indicating that aged brain ILC2 are in a deeper cell cycle quiescent state at homeostasis (Fig. 3 B). To determine whether ILC2 in the aged brain are capable of proliferating, we treated mice with 400 ng of IL-33, a known ILC2 activator, daily for 7 d (Fig. 3 C). Brain ILC2 from both young and aged mice vigorously proliferated in vivo in response to IL-33 (Fig. 3, D and E).

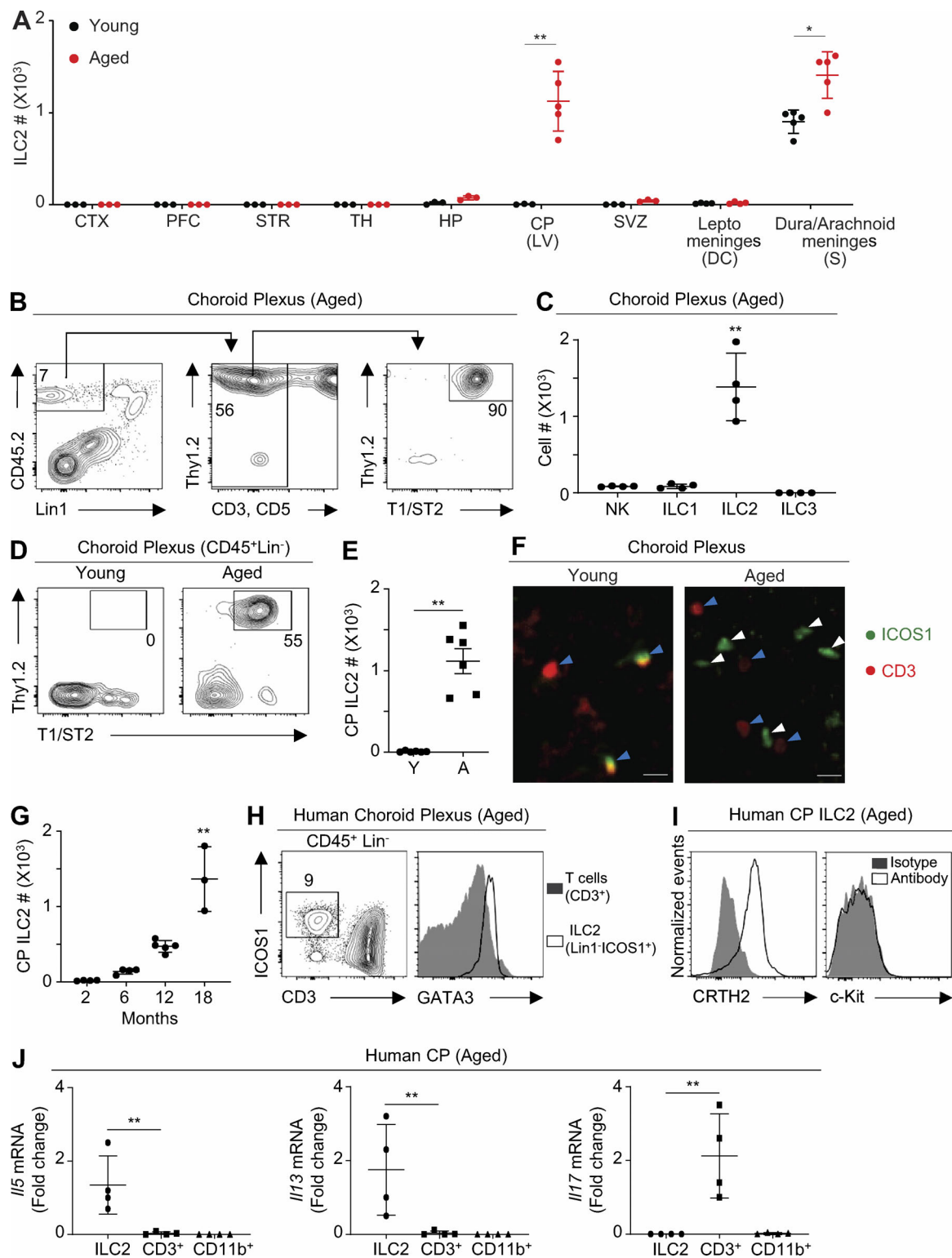


Figure 2. ILC2 accumulate in the CP of the aged brain. (A) Quantification of ILC2 numbers in different regions of young and aged mice. Data are from five mice per group, pooled from two independent experiments. CTX, cortex; PFC, prefrontal cortex; STR, striatum; TH, thalamus; SVZ, subventricular zone. CP lining the lateral ventricle (LV), leptomeninges attached to the brain parenchyma of dorsal cerebrum (DC), and dura/arachnoid meninges attached to the skull (S) were isolated. (B) Representative flow cytometry profiles of ILC2 in the CP of aged mice. (C) The number of various ILC subsets in the CP of aged mice. Data are four mice per group and are representative of two independent experiments. (D) Representative flow cytometry profiles of ILC2 in the CP of young and aged mice. (E) Quantification of ILC2 numbers in the CP of young (Y) and aged (A) mice. Data are from six mice per group, pooled from two independent experiments. (F) Representative whole-mount CP immunofluorescence staining profiles of ILC2 and T cells from young and aged mice. Scale bar length, 10 μ M. White arrowheads denote ILC2; blue arrowheads denote CD3⁺ T cells. Data represent six mice per group from two independent experiments. (G) Quantification of ILC2 numbers in the CP of mice at different ages. Data are from three or four mice per group and are representative of two independent experiments.

(H) Representative flow cytometry profiles of ILC2 in the CP of deceased elderly people >65 yr old. Data represent four autopsy samples. **(I)** Representative flow cytometry profiles depicting the expression of CRTH2 and cKit in human CP ILC2 from deceased elderly people. Data represent four autopsy samples. **(J)** mRNA levels of the indicated genes in sorted ILC2, CD3⁺ T cells, and CD11b⁺ myeloid cells in the CP tissue of deceased elderly people. Data are from four autopsy samples. Error bars are mean \pm SEM. *, $P < 0.05$; **, $P < 0.01$. Lin1 antibodies included anti-B220, anti-NK1.1, and anti-CD11b. Mouse total Lin antibodies included anti-B220, anti-NK1.1, anti-CD11b, anti-CD3, and anti-CD5. Human Lin1 antibodies included anti-CD56, anti-CD19, anti-CD11c, anti-CD11b, anti-CD14, and anti-FcyR1a.

The expansion of brain ILC2 at day 8 (24 h after the last IL-33 administration) as measured by the fold change over day 0 (naive mice) was similar between young and aged mice, indicating that the capability to respond to stimuli was preserved in aged brain ILC2 (Fig. 3, D and E). We then rested the mice for 4 wk and examined the cellularity of brain ILC2 again at day 36 (4 wk after the last IL-33 administration). ILC2 in the brains of young mice experienced notable contraction after activation, with a drop of about fourfold in cellularity at 4 wk after the withdrawal of IL-33 treatment (Fig. 3, D and E). ILC2 from aged brains, however, only experienced a very moderate contraction after activation, less than twofold reduction in cell number (Fig. 3, D and E). Thus, ILC2 in the aged brain are long-lived and relatively resistant to contraction after replication stress.

We then used 5-ethynyl-2'-deoxyuridine (EdU)-chasing experiments to better understand the longevity and persistence of ILC2 in the aged brain. More than half of the brain ILC2 were labeled with EdU during IL-33 treatment in both young and aged mice at day 8, verifying that aged brain ILC2 possess comparable proliferation capability as young brain ILC2 (Fig. 3 F). Interestingly, a large percentage of EdU⁺ ILC2 persisted in aged brains, but not in the brains of young mice, at 4 wk after the withdrawal of IL-33 treatment (Fig. 3 F). Thus, ILC2 in the aged brain are long-lived, persisting for a long period of time after the withdrawal of proliferation stimulus. Of note, the levels of EdU in ILC2 that persisted in aged brains after 4 wk were surprisingly high with a minute reduction over time, leading to the hypothesis that these cells may rapidly return to cell cycle quiescence after the withdrawal of replication stress (Fig. 3 F). Indeed, intracellular Ki67 staining suggested that ILC2 in aged brains, but not those in young mice, returned to cell cycle quiescence at 4 wk after IL-33 treatment (Fig. 3 G). Thus, ILC2 in the aged brain are capable of switching from proliferation to cell cycle dormancy after the withdrawal of replication stress. This capability may underlie their enhanced persistence after replication stress, because a return to cell cycle quiescence may protect these cells from DNA damage and other cellular insults. Indeed, ILC2 exhibited significantly lower caspase activity in the aged brain than in young mice at 3 wk after the withdrawal of IL-33 treatment, indicating reduced apoptosis (Fig. 3 H). Together, ILC2 in the aged brain were relatively resistant to contraction in response to replication stress.

We next determined whether the previously activated ILC2 in aged brains can respond to subsequent secondary stimulation. We treated aged mice with IL-33, rested them for 4 wk, and then readministered IL-33 or PBS daily for 2 d (Fig. 3, I–K). EdU diminished after readministration with IL-33, indicating that these cells had vigorously proliferated upon secondary stimulation, leading to the dilution of EdU (Fig. 3, I and J). Ki67

staining confirmed that ILC2 from aged brains indeed reentered cell cycle upon reactivation by IL-33 (Fig. 3, I and K). Thus, ILC2 in aged brains are able to reversibly switch between cell dormancy and proliferation, which may underlie their enhanced persistence and gradual accumulation with age.

The capability to reversibly switch between dormancy and cell cycle has also been observed in hematopoietic stem cells, which have the longest life span and most potent self-renewal potential (Wilson et al., 2008). We therefore used an in vitro culture assay to examine the self-renewal capability of ILC2 in the aged brain. ILC2 from the brains of both young and aged mice vigorously proliferated when cultured with IL-33 (Fig. 3 L). However, while ILC2 from the brains of young mice proliferated only up to 2 wk, ILC2 from aged brains proliferated for more than 4 wk without signs of exhaustion (Fig. 3 L). The growth of all cultures eventually slowed down to various degrees beyond 4 wk of culture (not shown). Hence, ILC2 from aged brains exhibited enhanced long-term self-renewal capability in vitro. The long-term cultured ILC2 from aged brains are functionally robust; they produced large amounts of the ILC2 signature cytokines IL-5 and IL-13 even after 4 wk of culture (Fig. 3 M). ILC2 in the aged brain exhibited similar functional capability as ILC2 in other organs (Fig. 3 M). They produced low amounts of the anti-inflammatory cytokine IL-10 (Fig. 3 M). They did not secrete IL-4 protein (Fig. 3 M), though mRNA for IL-4 was detected by RNA sequencing (RNA-Seq). They did not produce cytokines characteristic of alternative lymphocyte lineages, such as IL-17, IFN- γ , or IL-22, verifying that they were committed to the ILC2 lineage (Fig. 3 M). RNA-Seq indicated that ILC2 from aged brains can maintain high bioenergetics even under prolonged replication stress, as demonstrated by the high expression of oxidative phosphorylation genes at 2 wk of culture (Fig. 3 N). Consistent with their enhanced self-renewal capability, ILC2 from aged brains expressed high amounts of *Ascl2* and *Hif1a*, the transcription factors that promote stem cell self-renewal (Fig. 3, N and O). Interestingly, at 2 wk of culture, ILC2 isolated from aged brains expressed much lower levels of *Cdkn2a* (encoding P16) than their young counterparts, indicating that the P16-driven cellular senescence pathway may have been repressed in aged brain ILC2 (Fig. 3, N and O). *Cdkn2a* expression, however, eventually increased after 4 wk of culture, suggesting that the P16-driven cellular senescence pathway was delayed but not completely abolished in aged brain ILC2 (Fig. 3 O). Compared with young brain ILC2, ILC2 from aged brains also had remarkably lower expression of the lymphocyte exhaustion marker *Havcr2*, and the expression remained low over time in culture, indicating that lymphocyte exhaustion may also be suppressed in aged brain ILC2 (Fig. 3, N and O).

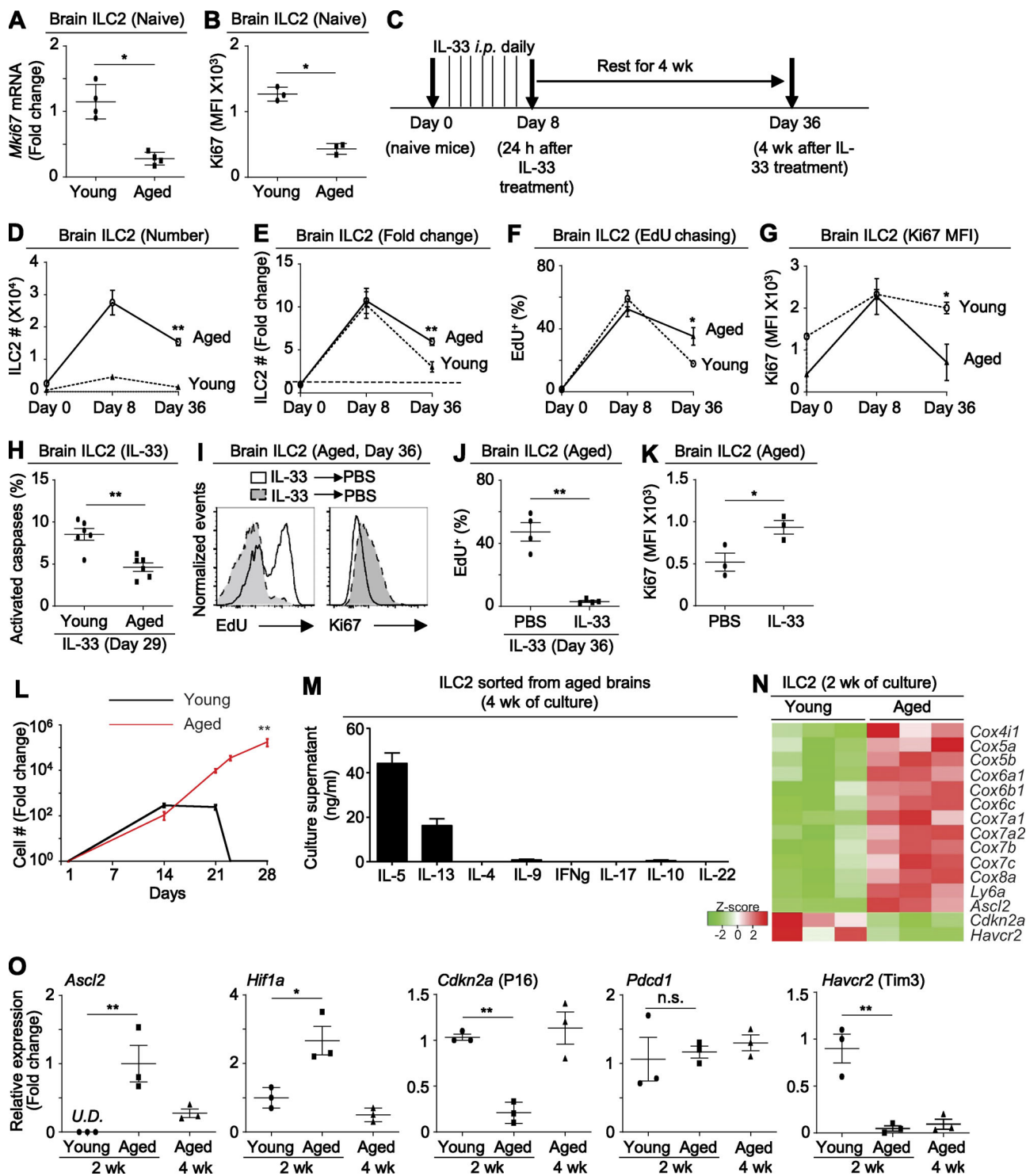


Figure 3. ILC2 in the aged brain are long-lived, capable of switching between cell cycle quiescence and proliferation, and relatively resistant to cellular senescence and exhaustion. (A) mRNA expression of *Mki67* (encoding Ki67) in ILC2 sorted from the brains of young and aged mice. Data are from four mice per group and are representative of two independent experiments. (B) Mean fluorescence intensity (MFI) of Ki67 in ILC2 from young and aged mice, assessed by intracellular staining and flow cytometry analysis. Data are from three mice per group and are representative of two independent experiments. (C) Schematic for IL-33 injections in D–G. Young or aged mice were administrated with IL-33 daily for 7 d. Brain ILC2 in young and aged mice were examined at day 0 (naive mice), day 8 (24 h after the last IL-33 administration), and day 36 (4 wk after the last IL-33 administration). (D) Quantification of brain ILC2 numbers at day 0, day 8, and day 36. Data are from three to seven mice per group and are representative of two independent experiments. (E) Fold change of brain ILC2 numbers at day 0, day 8, and day 36. The average ILC2 number at day 0 was arbitrarily set as 1. Data are from three to seven mice per group and are representative of two independent experiments. (F) EdU was administrated simultaneously with IL-33 treatment. EdU concentrations in ILC2 were measured at day 0 (naive mice), day 8 (24 h after the last EdU/IL-33 administration), and day 36 (4 wk after the last EdU/IL-33 administration). Percentages of EdU+ brain ILC2 at day 0, day 8, and day 36. Data are from three to seven mice per group and are representative of two independent experiments. (G) MFI of Ki67 in brain

ILC2 at day 0, day 8, and day 36. Data are from three to seven mice per group and are representative of two independent experiments. **(H)** Percentage of ILC2 that expressed activated caspases at day 29. Data are from six mice per group, pooled from two independent experiments. **(I)** Aged mice were treated with IL-33 for 7 d together with EdU. The mice were then rested for 4 wk and administrated with IL-33 or PBS again for 2 d. EdU concentrations were measured at 7 d after secondary injections with IL-33 or PBS. Ki67 expression was measured at 24 h after secondary injections with IL-33 or PBS. **(J)** Percentages of EdU⁺ ILC2 at 7 d after secondary injection of IL-33 or PBS. Data are from three mice per group and are representative of two independent experiments. **(K)** MFI of Ki67 in aged brain ILC2 at 24 h after secondary injections with IL-33 or PBS. Data are from three mice per group and are representative of two independent experiments. **(L)** ILC2 from the brains of young and aged mice were sorted and cultured with IL-7, IL-2, IL-33, and SCF for up to 4 wk. Fold change of cell numbers over time is shown. Data are from three mice per group and are representative of three independent experiments. **(M)** Cytokine concentrations in the culture supernatant of ILC2 isolated from aged brains and cultured *in vitro* for 4 wk. Data are from three mice per group and are representative of two independent experiments. **(N)** Heatmap depicts the expression of representative genes by RNA-Seq comparing ILC2 isolated from the brains of young versus aged mice and cultured for 2 wk *in vitro*. **(O)** qPCR showing the expression of the indicated genes in ILC2 isolated from the brains of young and aged mice and cultured for 2 or 4 wk *in vitro*. Data are from three mice per group and are representative of two independent experiments. Error bars are mean \pm SEM. *, $P < 0.05$; **, $P < 0.01$. n.s., not significant; U.D., undetectable.

Together, ILC2 from the aged brain are relatively resistant to cellular senescence and exhaustion, which may lead to enhanced long-term self-renewal capability.

ILC2 in aged brains are functionally quiescent at homeostasis but can produce large amounts of IL-5 and IL-13 *in vivo* in response to exogenous stimuli

We next sought to investigate how aging affects brain ILC2 functionality. ILC2 are known to produce basal levels of cytokines at homeostasis (Nussbaum et al., 2013). Using intracellular cytokine staining, we detected the expression of IL-5 and IL-13 in brain ILC2 in naive young mice (Fig. 4, A and B). However, ILC2 in aged brains had markedly reduced expression of both IL-5 and IL-13 at homeostasis (Fig. 4, A and B). Thus, not only are aged brain ILC2 in deep cell cycle dormancy, but they are also functionally quiescent in homeostatic states.

We next examined whether ILC2 from aged brains can be activated to produce cytokines in response to exogenous stimuli. Indeed, brain ILC2 from both young and aged mice produced large amounts of IL-5 and IL-13 in response to *in vivo* IL-33 treatment (Fig. 4, C and D). The production of IL-5 and IL-13 by brain ILC2 was comparable between IL-33-treated young and aged mice (Fig. 4, C and D). Hence, despite functional quiescence at homeostasis, ILC2 in the aged brain have preserved potent functional capability to respond to exogenous stimuli.

To understand whether ILC2 activation may influence the cognitive function of aged mice, we used an established Object Placement Test to examine spatial recognition (Zuloaga et al., 2016). Mice were allowed to explore two identical objects placed in a box. After 24 h, one of the objects was moved to a new location (displaced object), and mice were allowed to explore the familiar and the displaced objects (Fig. 4 E). Young mice spent the majority of the time exploring the displaced object, whereas aged mice showed no preference between the two objects, indicating a loss of spatial recognition with aging (Fig. 4 F). We next examined whether IL-33 treatment may influence the cognitive function of aged mice. IL-33 treatment did not significantly affect the overall motor capability of aged mice (Fig. 4 G). IL-33-treated aged mice, however, spent significantly more time interacting with the displaced object over the familiar one in the Object Placement Test, suggesting improved spatial recognition (Fig. 4 H). Thus, ILC2 activation may be associated with improved cognitive function in aged mice.

Activated ILC2 can improve the cognitive function of aged mice

To directly examine whether activated ILC2 can improve the cognitive function of aged mice, we sorted ILC2 from aged brains and expanded and activated them *in vitro* with stem cell factor (SCF), IL-7, IL-2, and IL-33. We then transferred the *in vitro* activated ILC2 into the brains of aged mice by *i.c.v.* injection. Transfer of activated ILC2 did not significantly affect the overall motor capability of aged mice (Fig. 5 A). Interestingly, transfer of activated ILC2 drastically enhanced cognitive function of aged mice during the Object Placement Test (Fig. 5 B). We additionally performed the Morris Water Maze Test, in which aged mice exhibited reduced spatial memory (Fig. S2 A). The Morris Water Maze Test verified that aged mice, which received *i.c.v.* transfer of activated ILC2, displayed significantly enhanced spatial memory, as demonstrated by an increased percentage of time spent in the target quadrant as well as increased number of entries into the target zone during the probe trial (Fig. 5 C). Together, these data provide direct evidence that activated ILC2 can improve the cognitive function of aged mice.

To explore the molecular mechanisms by which activated ILC2 lead to improved cognitive function in aged mice, we performed RNA-Seq to compare the transcriptomes of ILC2, CD3⁺ T cells, and microglia in the brains of IL-33-treated aged mice. While microglia in aged brains displayed great transcriptomal heterogeneity, ILC2 in aged brains were relatively homogeneous and transcriptionally close to T cells (Fig. 5 D). Around 3,000 genes were differentially expressed between ILC2 and microglia, and ~700 differentially expressed genes between ILC2 and T cells were identified (Fig. 5, E and F). Genes differentially expressed between ILC2 and microglia were enriched for effector molecules including cytokines, cell adhesion molecules, and phagocytosis genes (Fig. 5 G). Similarly, genes differentially expressed between ILC2 and T cells were also overrepresented by effector molecules such as cytokines, chemokines, and cell adhesion molecules (Fig. 5 G). By overlapping the two lists of differentially expressed genes, we identified 161 genes that were highly expressed by ILC2, but not by T cells or microglia, in the brains of IL-33-treated aged mice (Fig. 5, H–J). Notably, these 161 genes were enriched for cytokines/cytokine receptor genes and chemokine signaling molecules, as well as hippo signaling, suggesting ILC2 in aged brains may possess unique functional capability (Fig. 5 H).

In addition to IL-5 and IL-13, ILC2 in aged brains also expressed high amounts of several growth factors that may

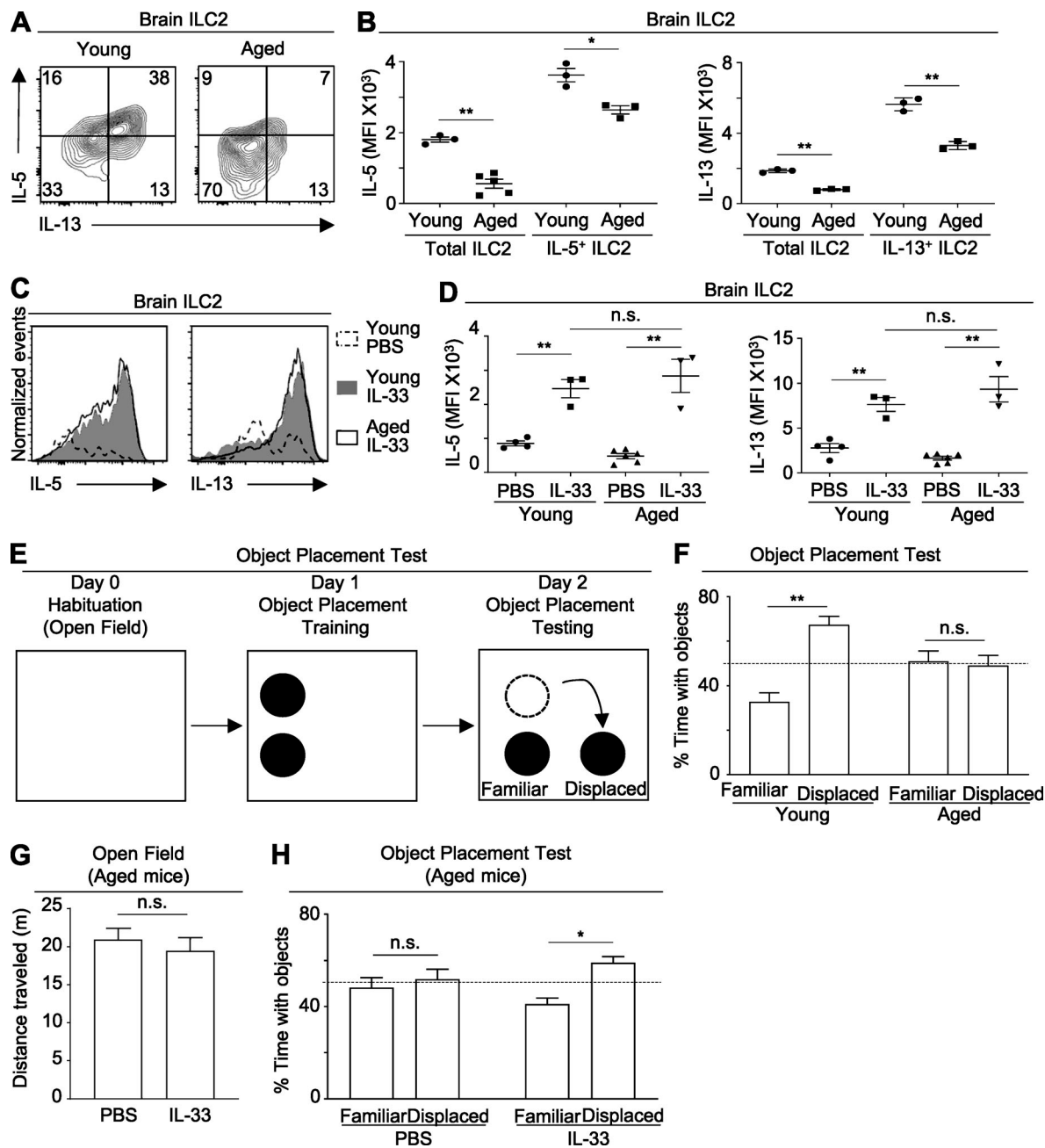


Figure 4. ILC2 in the aged brain are functionally dormant at homeostasis but can be activated by IL-33 to produce large amounts of type 2 cytokines in vivo. (A) Representative flow cytometry profiles showing the expression of IL-5 and IL-13 by brain ILC2 in young versus aged mice at homeostasis. (B) MFI of IL-5 and IL-13 by total brain ILC2 or cytokine-expressing ILC2 in young versus aged mice at homeostasis. Data are from three mice per group and are representative of three independent experiments. (C) Representative flow cytometry profiles of the expression of IL-5 and IL-13 by brain ILC2 in young or aged mice treated with IL-33 or PBS daily for 7 d. (D) MFI of IL-5 and IL-13 expressed by brain ILC2 in young or aged mice treated with IL-33 or PBS daily for 7 d. Data are from three to six mice per group and are representative of two independent experiments. (E) Experimental scheme for the Object Placement Test. (F) Percentage of time spent with familiar or displaced objects for young and aged mice. Data are from 9 or 10 mice per group and are representative of two independent experiments. (G) Distance traveled by aged mice treated with IL-33 or PBS in the Open Field Test. Data are from 9–14 mice per group and are representative of two independent experiments. (H) Percentage of time spent with familiar or displaced objects for aged mice treated with IL-33 or PBS daily for 2 d. Data are from 9–14 mice per group and are representative of two independent experiments. Error bars are mean \pm SEM. *, $P < 0.05$; **, $P < 0.01$. n.s., not significant.

promote neural survival, stimulate neurogenesis, or enhance lymphatic drainage (Fig. 5, I and J). They included known ILC2 products such as *Areg*, *Arg1*, and *Bmp7*, as well as previously unreported effector molecules such as *Vegfc* and *Lif* (Fig. 5, I and J;

Brombacher et al., 2017; Chen and Trapp, 2016; Da Mesquita et al., 2018; Davis and Pennypacker, 2018; de Rivero Vaccari et al., 2009; Ito et al., 2019; Kiyota et al., 2018; Monticelli et al., 2016; Nussbaum et al., 2013; Robinette et al., 2015). A number of

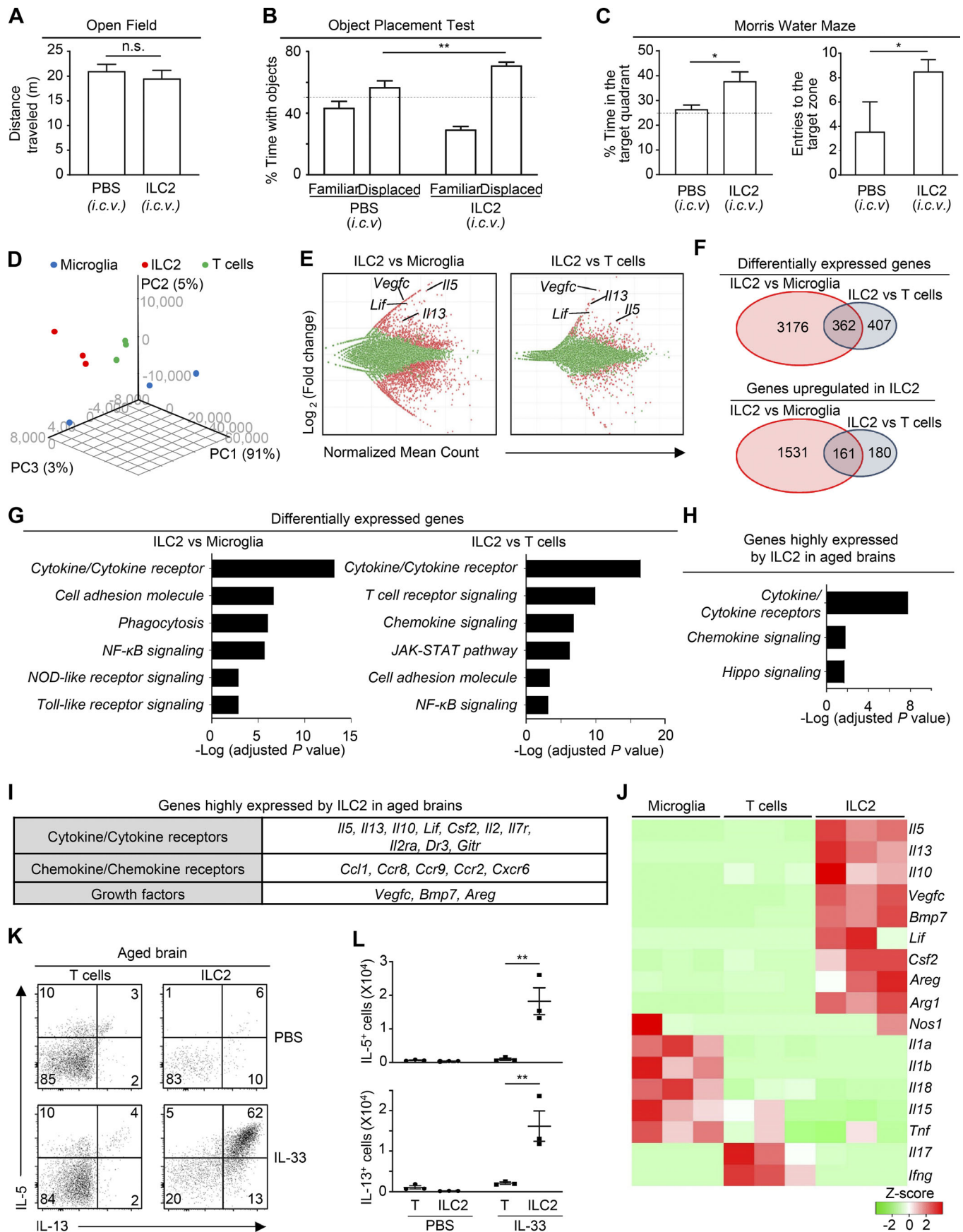


Figure 5. Activated ILC2 improve cognitive function in aged mice. (A) ILC2 were isolated from brains of aged mice and cultured in vitro with IL-33, IL-2, IL-7, and SCF for 4 wk. The Object Placement Test was performed with aged mice that received i.c.v. injection of 2×10^5 in vitro expanded and activated brain ILC2 or PBS. Mice were rested for 1 wk after surgery before behavior testing. Distance traveled in the Open Field Test was quantified. Data are from 8–11 mice per group, pooled from two independent experiments. (B) Percentage of time spent with familiar or displaced objects in the Object Placement Test. Data are from 8–11 mice per group, pooled from two independent experiments. (C) The Morris Water Maze was performed with mice that were i.c.v. injected with in vitro expanded and activated brain ILC2 or PBS. Percentage of time spent in the target quadrant and the number of entries to the target zone were quantified. Data are from 9–11 mice per group, pooled from two independent experiments. (D) RNA-Seq was performed with sorted microglia, ILC2, or T cells from the brains of aged mice treated with IL-33 daily for 7 d. Principal component analysis was performed. (E) MA (log-ratio versus mean log-expression) plots comparing the gene expression profiles. (F) Venn diagrams depicting the numbers of differentially expressed genes. (G) Pathway analysis of differentially expressed genes. (H) Pathway analysis of genes that are highly expressed in brain ILC2 but not in microglia or brain T cells of IL-33-treated aged mice. (I) List of effector molecules, receptors, and transcription factors that are highly expressed in brain ILC2 of IL-33-treated aged mice. (J) Heatmap depicts the expression of effector molecules expressed by different immune cell subsets in the brains of IL-33-treated aged mice. (K) Representative flow cytometry profiles of IL-5 and IL-13 expression by brain T cells or ILC2 in PBS- or IL-33-treated aged mice. (L) Quantification of the number of IL-5- or IL-13-producing brain T cells and ILC2 in IL-33-treated aged mice. Data are from three mice per group and are representative of two independent experiments. Error bars are mean \pm SEM. *, $P < 0.05$; **, $P < 0.01$. n.s., not significant.

pro-inflammatory cytokines, such as *Il1a*, *Il1b*, *Il18*, *Il15*, and *Tnf*, were highly expressed by microglia in the aged brain (Fig. 5 J). Genes indicating a reparative phenotype, such as *Arg1* and *Nos1*, were not significantly expressed in aged microglia even after IL-33 treatment. T cells in the aged brain were biased toward Th1 and Th17 phenotypes (Fig. 5 J). Expression of type 2 cytokines was nearly undetectable in aged brain T cells (Fig. 5 J). Flow cytometry analysis verified that T cells in aged brains failed to produce a significant amount of type 2 cytokines IL-5 or IL-13 in response to IL-33 (Fig. 5, K and L). Together, aged brain ILC2 exhibited a unique transcriptomal profile and were the predominant source of type 2 cytokines as well as a number of other effector molecules in response to IL-33.

CP ILC2 possess more potent capability to proliferate and to produce type 2 cytokines than meningeal ILC2.

We next examined the anatomical distribution of ILC2 in the brains of IL-33-treated aged mice. I.v. anti-CD45.2 PE labeling revealed that ILC2 might proliferate locally in the brain in both young and aged mice following IL-33 treatment (Fig. S3, A and B). ILC2 remained enriched in the CP of aged mice following IL-33 treatment, although a significant amount of ILC2 was also detected in the meninges of IL-33-treated aged mice (Fig. 6 A). We next compared the proliferative and functional capabilities of meningeal and CP ILC2. We first sorted ILC2 and cultured them with IL-2, IL-7, IL-33, and SCF in vitro (Fig. 6 B). Interestingly, both meningeal and CP ILC2 isolated from aged mice, but not meningeal ILC2 from young mice, proliferated for more than 4 wk (Fig. 6 B). Thus, the resistance to cellular senescence might be conferred by aging, regardless of the specific anatomical sites in the brain. Nevertheless, compared with meningeal ILC2, CP ILC2 in aged mice appeared to proliferate more rigorously in vitro (Fig. 6 B).

We then compared the in vivo proliferative and functional capabilities of meningeal and CP ILC2 in aged mice (Fig. 6, C–F). Indeed, compared with meningeal ILC2, CP ILC2 possessed much more potent capability to proliferate in vivo in response to IL-33 (Fig. 6, C and D). The number of CP ILC2 increased more than sevenfold in response to IL-33 treatment, whereas the number of meningeal ILC2 increased only around twofold (Fig. 6, C and D). CP ILC2 in IL-33-treated aged mice also expressed higher

amounts of both IL-5 and IL-33 than meningeal ILC2 did (Fig. 6, E and F). Of note, meningeal and CP ILC2 from aged mice expressed comparable amounts of *Il1rl1* (encoding IL-33R), indicating that other mechanisms underlie their functional difference (Fig. S3, C and D). Together, CP ILC2 possess more potent capability to proliferate and to produce type 2 cytokines in response to IL-33 than meningeal ILC2.

We next performed single-cell RNA-Seq (scRNA-Seq) to compare the transcriptomes of meningeal ILC2 and CP ILC2 in IL-33-treated aged mice. The purpose of IL-33 treatment was to better assess the functional capability of ILC2. We first examined the merged population consisting of both meningeal and CP ILC2. We identified three distinct ILC2 subsets in IL-33-treated aged mice using Uniform Manifold Approximation and Projection (UMAP; Fig. 6 G). We named these three subsets ILC2_{A1}, ILC2_{A2}, and ILC2_{A3} (Fig. 6 G). ILC2_{A2} expressed lower amounts of type 2 cytokines as well as other effector molecules than the other subsets and therefore may represent a relatively inactive subset (Fig. 6 H). ILC2_{A1} and ILC2_{A3} represented two activated ILC2 subsets with distinct transcriptional profiles (Fig. 6, G and H). Notably, ILC2_{A1} expressed higher amounts of *Arg1* and *Il13*, whereas ILC2_{A3} expressed higher amounts of *Csf2* (Fig. 6 H). *Gata3* expression was comparable among all three subsets (Fig. 6 H).

We next compared the single-cell transcriptomes between meningeal ILC2 and CP ILC2. Interestingly, CP ILC2 contained a higher proportion of ILC2_{A1}, whereas meningeal ILC2 contained a higher proportion of ILC2_{A3} (Fig. 6, I and J). Consistent with this pattern, CP ILC2 expressed higher amounts of *Il13*, and meningeal ILC2 expressed higher amounts of *Csf2* (Fig. 6 K). CP ILC2 also expressed higher amounts of *Il5* than meningeal ILC2 did (Fig. 6 K). In particular, although meningeal ILC2 had an increased proportion of the ILC2_{A3} subset, meningeal ILC2_{A3} expressed significantly lower amounts of multiple effector molecules, including *Il5*, *Il13*, *Lif*, and *Ccl1* than the CP ILC2_{A3} (Fig. 6 L). Thus, meningeal ILC2 had a reduced proportion of ILC2_{A1} cells and their ILC2_{A3} subset also exhibited a less activated phenotype than CP counterparts, leading to reduced cytokine-producing activity compared with CP ILC2.

Notably, all subsets of CP ILC2 expressed markedly higher amounts of the urea cycle enzyme *Arg1* than the meningeal ILC2

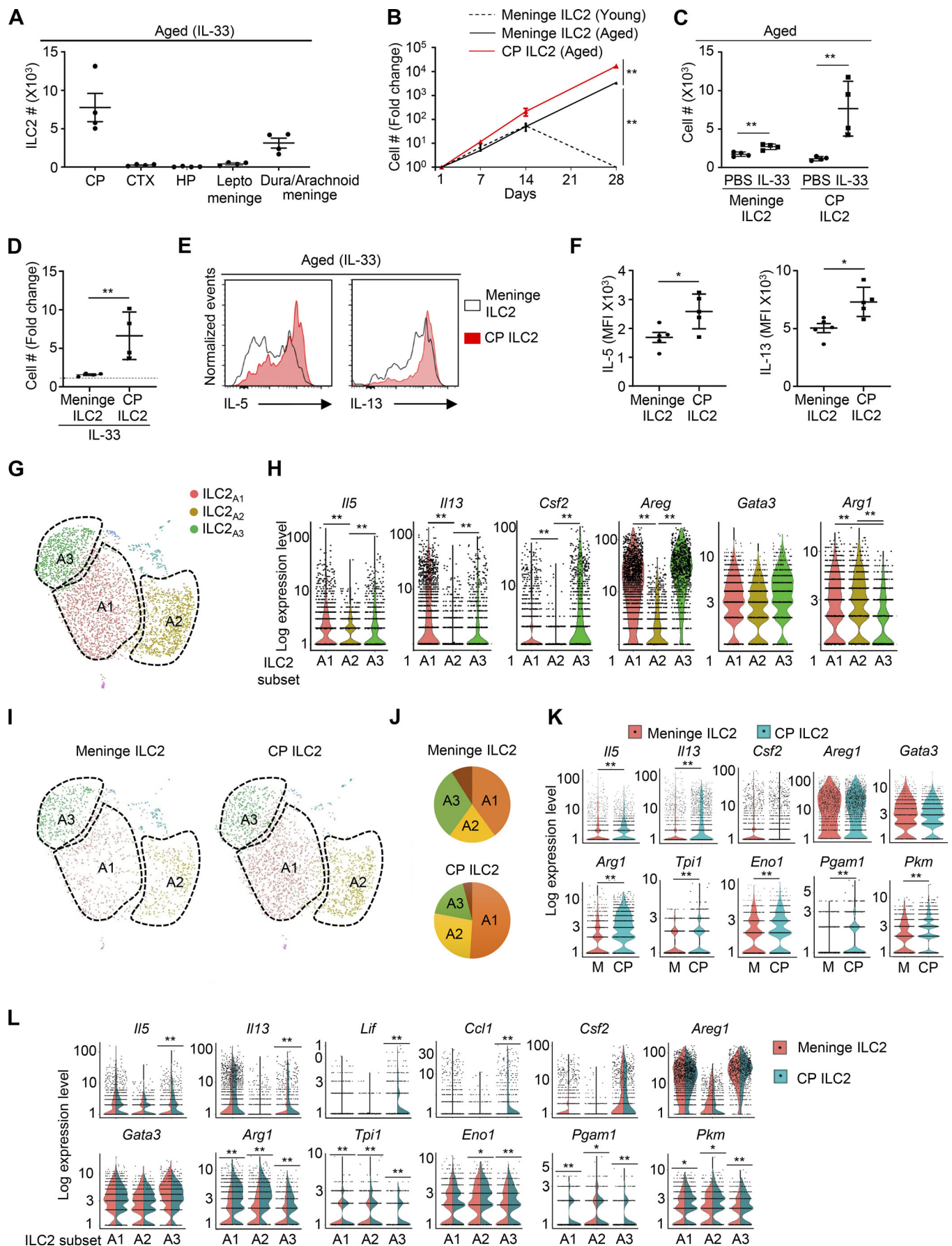


Figure 6. CP ILC2 possess more potent proliferative and cytokine-producing capability than meningeal ILC2 in aged mice. (A) Number of ILC2 at different regions of aged mice after daily IL-33 treatment for 7 d. Data are from four mice per group and are representative of two independent experiments. CTX, cortex. (B) ILC2 from the meninges of young mice and the meninges of aged mice and CP from aged mice were sorted and cultured with IL-7, IL-2, IL-33, and SCF for up to 4 wk. Fold change of cell numbers over time is shown. Data are from four mice per group and are representative of two independent experiments. (C) Numbers of meningeal and CP ILC2 in aged mice treated with PBS or IL-33 daily for 7 d. Data are from four mice per group and are representative of two independent experiments. (D) Fold change of ILC2 numbers in IL-33-treated mice over those in PBS-treated mice. The average ILC2 number in PBS-treated mice was set as 1. Data are from four mice per group and are representative of two independent experiments. (E) Representative flow cytometry profiles of IL-5 and IL-13 expression in meningeal and CP ILC2 in IL-33-treated aged mice. (F) MFI of IL-5 and IL-13 in meningeal and CP ILC2 in IL-33-treated aged mice. Data are from five mice per group and are representative of two independent experiments. (G) scRNA-Seq was performed with sorted meningeal and CP ILC2 from IL-33-treated aged mice. UMAP analysis of the combined ILC2 and meningeal ILC2 population. (H) Expression of the indicated genes by different subsets of ILC2 in the combined meningeal and CP ILC2 population. (I) Split analysis of meningeal and CP ILC2 by UMAP. (J) Percentage of each ILC2 subset in meningeal and CP ILC2. (K) Expression of the indicated genes by meningeal and CP ILC2. (L) Expression of the indicated genes in each ILC2 subset in meningeal and CP ILC2. Error bars are mean \pm SEM. *, $P < 0.05$; **, $P < 0.01$.

subsets (Fig. 6, K and L). Previous work indicated that *Arg1* may control the glycolysis of activated ILC2 (Bando et al., 2013; Monticelli et al., 2016). Indeed, CP ILC2 expressed higher amounts of multiple essential glycolytic enzyme genes than meningeal ILC2, suggesting enhanced glycolysis (Fig. 6, K and L). These genes included *Tpi1* (encoding triosephosphate isomerase 1), *Eno1* (encoding α -enolase), *Pgam1* (encoding phosphoglycerate mutase 1), and *Pkm* (encoding pyruvate kinase; Fig. 6, K and L). The increased expression of *Arg1* and glycolytic enzyme genes likely underlies the enhanced proliferative and cytokine-producing capability of CP ILC2.

Recent work indicates that ILC2 in distinct organs express different levels of cytokine receptor, which may be related to their differential developmental origins (Ricardo-Gonzalez et al., 2018; Schneider et al., 2019). We therefore examined the gene expression of various cytokine receptors in meningeal and CP ILC2. Quantitative PCR (qPCR) and scRNA-Seq data revealed that both meningeal and CP ILC2 in aged mice expressed high amounts of *Il1r1* (encoding IL-33R), but not *Il17rb* (encoding IL-25R) or *Il18r1* (Fig. S3, C and D). Thus, the cytokine receptor expression patterns of aged meningeal and CP ILC2 most closely resemble those of lung and adipose ILC2.

Together, ILC2 in the CP of aged mice possess enhanced capability to proliferate and to produce type 2 cytokines in response to IL-33. In addition, activated CP ILC2 in aged mice exhibited a unique transcriptome pattern that might reflect a distinctive functional capability and metabolism pathway.

IL-5 improves the cognitive function of aged mice

To understand the specific effector molecules by which activated ILC2 enhance cognitive function in aged mice, we administered recombinant IL-5 or IL-13 to aged mice. IL-13 has been shown to promote spatial learning and memory in young mice (Brombacher et al., 2017), whereas whether IL-5 affects cognitive function remains unknown. Surprisingly, administration of IL-5, but not IL-13, improved the cognitive function of aged mice in the Object Placement Test (Fig. 7 A). The Morris Water Maze test verified that IL-5-treated aged mice had enhanced spatial learning and memory, as demonstrated by the higher percentage of time spent in the target quadrant (Fig. 7 B). IL-5 treatment did not significantly affect the general motor capability of aged mice (Fig. S2 B). IL-5 treatment also did not significantly alter spatial recognition of young mice (Fig. S2, C and D). Together, IL-5 but

not IL-13 was sufficient to improve cognitive function in aged mice.

We sought to understand whether activated ILC2 can alleviate aging-associated cognitive decline through the production of IL-5. We attempted to delete IL-5 in activated ILC2 using lenti-CRISPRv2-GFP knockout vectors (Walter et al., 2017). Nevertheless, ILC2 from the aged brain were resistant to lentiviral transduction in vitro (Fig. S4 A). We therefore used the ILC2/b6 cell line, an immortalized ILC2 line derived from small intestinal lamina propria (Shen et al., 2019; Zhang et al., 2017). Similar to ILC2 in the aged brains, the ILC2/b6 cell line vigorously proliferated and produced large amounts of IL-5 and IL-13 in vitro, and they lacked the production of alternative lineage effector molecules such as IL-17 or IFN- γ (Shen et al., 2019; Zhang et al., 2017). We cultured and activated ILC2/b6 cells in vitro and efficiently deleted IL-5 in ILC2/b6 cells using the lenti-CRISPRv2-GFP construct containing a guide RNA (gRNA) sequence that targeted IL-5 (Fig. S4 B). Non-target control (NTC) gRNA was used as control (Fig. S4 B). We then transferred activated IL-5-deficient or control ILC2/b6 cells into aged mice by i.c.v. injection (Fig. 7 C). Notably, transfer of control ILC2/b6 cells, but not IL-5-deficient ILC2/b6, significantly enhanced spatial recognition of aged mice in the Object Placement Test (Fig. 7 C). Thus, activated ILC2 may alleviate aging-associated cognitive decline through the production of IL-5.

We next examined whether IL-33 can improve the cognitive function of aged mice through IL-5-dependent mechanisms. We treated aged mice with IL-33 together with i.c.v. injection of anti-IL-5 neutralizing antibody or isotype control (Fig. 7 D). Anti-IL-5 treatment reduced the cognitive function of IL-33-treated aged mice, suggesting that IL-33 might alleviate aging-associated cognitive decline through IL-5-dependent mechanisms (Fig. 7 D). Together, our results highlight a novel role for IL-5 in alleviating aging-associated cognitive decline.

We sought to understand the mechanisms by which IL-5 promotes the cognitive function of aged mice. Compared with PBS treatment, IL-5 treatment increased the number of EdU⁺ cells at the dentate gyrus (DG) region of the HP following in vivo EdU labeling, indicating enhanced HP neurogenesis (Fig. 7 E). Because reduced neuroinflammation is often associated with enhanced neurogenesis and improved cognitive function, we performed RNA-Seq to examine the transcriptome changes in brain-resident T cells and microglia, two major sources of

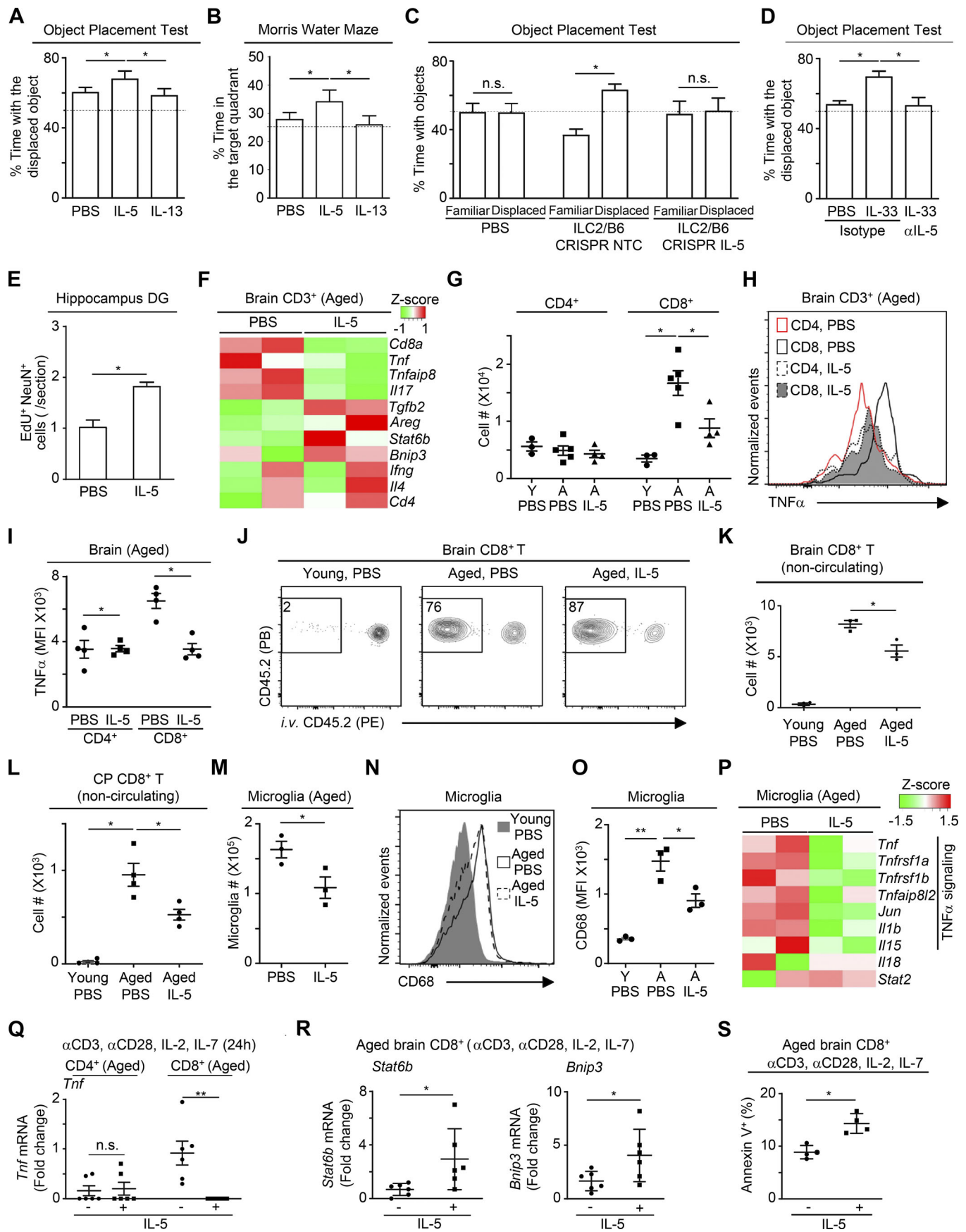


Figure 7. IL-5 improves the cognitive function in aged mice. (A) The Object Placement Test was performed with aged mice after injection of IL-5, IL-13, or PBS daily for 2 d. Percentage of time spent with the displaced objects was quantified. Data are from 9 or 10 mice per group and are representative of two independent experiments. (B) The Morris Water Maze test was performed with aged mice after PBS, IL-5, or IL-13 treatment for 2 d. Percentage of time spent in the target quadrant was quantified. Data are from 9 or 10 mice per group and are representative of two independent experiments. (C) IL-5 was deleted in activated ILC2/b6 cells using the CRISPR-mediated gene knockout technique. The Object Placement Test was performed with aged mice 1 wk after i.c.v injection with control or IL-5-deficient ILC2/b6 cells. Percentage of time spent with displaced objects was quantified. Data are from 9 or 10 mice per group, pooled from two independent experiments. (D) Aged mice received i.c.v injection of 10 μ g anti-IL-5 antibody or isotype control, followed by i.p. injection of IL-33 or PBS daily for 2 d. The Object Placement Test was performed after 1 wk of i.c.v injection. Percentage of time spent with the displaced objects was quantified. Data are from 8–11 mice per group, pooled from two independent experiments. (E) IL-5- or PBS-treated aged mice were injected with EdU in vivo. EdU⁺ cells in the HC DG regions was examined and quantified by immunofluorescence at 2 d after the last dose of IL-5 or PBS treatment. Data are from four mice per group. (F) Heatmap depicts the gene expression profiles of CD3⁺ T cells from the brains of PBS- or IL-5-treated aged mice by RNA-Seq. (G) Numbers of CD4⁺ and CD8⁺ T cells in the brains of young (Y) or aged (A) mice treated with PBS or IL-5. Data are from four mice per group and are representative of three independent experiments. (H) Representative flow cytometry profiles of TNF α expression by CD4⁺ or CD8⁺ T cells in the brains of aged mice treated with PBS or IL-5. (I) MFI of TNF α in brain CD4⁺ or CD8⁺ T cells of aged mice treated with PBS or IL-5. Data are from three to five mice per group and are representative of three independent experiments. (J) Representative flow cytometry profiles of CD8⁺ cells in the brains of aged mice that were injected i.v. with anti-CD45.2 PE antibody and euthanized 3 min later. PB, pacific blue. (K) The number of noncirculating brain CD8⁺ T cells that were not labeled with i.v. injected anti-CD45.2 antibody. Data are from three mice per group and are representative of two independent experiments. (L) The number of noncirculating CD8⁺ T cells in the CP of young or aged mice treated with PBS or IL-5. Data are from four mice per group and are representative of two independent experiments. (M) The number of microglia in IL-5- or PBS-treated aged mice. Data are from three mice per group and are representative of two independent experiments. (N) Representative flow cytometry profiles of CD68 expression by microglia in IL-5- or PBS-treated aged mice. (O) MFI of CD68 on microglia of IL-5- or PBS-treated aged mice. Data are from three mice per group and are representative of two independent experiments. (P) Heatmap depicts the gene expression profiles of microglia from PBS- or IL-5-treated aged mice by RNA-Seq. (Q) CD4⁺ or CD8⁺ T cells from the brains of aged mice were sort-purified and cultured in the presence or absence of IL-5 for 24 h. *Tnf* expression was examined by qPCR. Data are from six mice per group and are representative of two independent experiments. (R) Expression of the indicated genes in CD8⁺ T cells sorted from the aged brain and cultured in the presence or absence of IL-5 for 24 h. Data are from six mice per group and are representative of two independent experiments. (S) Annexin V staining was performed at 3 d of culture. Data are from four mice per group and are representative of two independent experiments. Error bars are mean \pm SEM. *, $P < 0.05$; **, $P < 0.01$. n.s., not significant.

pro-inflammatory cytokines in the aged brain. Notably, in vivo IL-5 treatment reduced the expression of the pro-inflammatory cytokine *Tnf* in CD3⁺ T cells of the aged brain (Fig. 7 F). Because elevated TNF α levels are known to impair neurogenesis and cognitive function (Faraco et al., 2018; Habbas et al., 2015; Liu et al., 2014; Terrando et al., 2010), the reduced expression of *Tnf* likely contributes to improved learning and memory in IL-5-treated aged mice. In contrast, the expression of anti-inflammatory growth factors, including *Tgfb2* and *Areg*, was increased by IL-5 treatment in T cells of the aged brain (Fig. 7 F). The expression of Th1 and Th2 characteristic molecules, including *Ifng* and *Il4*, respectively, was not significantly altered by IL-5 treatment (Fig. 7 F). The expression of T reg cell characteristic genes *Il10* and *Foxp3* was barely detectable.

We next performed flow cytometry analysis to examine the number and cytokine production of T cells in the aged brain. Notably, aging leads to the accumulation of CD8⁺ T cells that produced high amounts of TNF α , and IL-5 treatment reduced the number as well as TNF α expression of CD8⁺ T cells in the aged brain (Fig. 7, G–I). In contrast, IL-5 treatment did not significantly alter the number or TNF α expression of CD4⁺ T cells in aged mice (Fig. 7, G–I). I.v. labeling of anti-CD45.2 antibody revealed that the majority of CD8⁺ T cells that accumulated in the aged brain were noncirculating, tissue-resident cells (Fig. 7, J and K). In particular, tissue-resident CD8⁺ T cells drastically accumulated in the CP of aged mice, and their number was reduced by IL-5 treatment (Fig. 7 L). Together, IL-5 treatment restrains T cell inflammation, especially TNF α expression, which may lead to improved neurogenesis and enhanced cognitive function of the aged brain.

TNF α may also induce myeloid cells to produce neuro-destructive pro-inflammatory molecules, such as TNF α itself,

IL-1 β , and IL-15 (Di Paolo et al., 2015; Pan et al., 2009; Yarinina et al., 2008). We therefore also examined microglia in IL-5-treated aged mice. Microglia in IL-5-treated aged mice were moderately reduced in numbers and exhibited a less activated phenotype as demonstrated by reduced surface CD68 expression (Fig. 7, M–O). RNA-Seq revealed that microglia in IL-5-treated aged mice had an extensive reduction in the expression of TNF α signaling molecules, including TNF α receptors and downstream signaling molecules and transcriptional regulators (Fig. 7 N). The expression of TNF α -induced pro-inflammatory cytokines, including TNF α itself, *Il-1b*, and *Il-15*, was also reduced in aging microglia after in vivo IL-5 treatment (Fig. 7 N). The expression of TNF α -independent pro-inflammatory signaling molecules, such as *Il18* and *Stat2*, was not significantly reduced by IL-5 treatment (Fig. 7 N). Together, IL-5 also reduced microglia inflammation, possibly by decreasing TNF α signaling.

We next sought to understand the mechanism by which IL-5 restrains neuroinflammation in the aged brain. IL-5 was found to induce proliferation of regulatory eosinophils that can repress tissue inflammation (Andersson et al., 2014; Arnold et al., 2018; Finlay et al., 2016; Lingblom et al., 2017; Mesnil et al., 2016). However, eosinophils were not detected in the brains of aged mice after in vivo IL-5 treatment, indicating that other mechanisms might be involved (Fig. S5 A). We noted that, in response to in vivo IL-5 treatment, CD3⁺ T cells in the aged brain exhibited increased expression of IL-5 signaling molecule *Stat5b* and IL-5-induced apoptotic molecule *Bnip3*, leading to the hypothesis that IL-5 might directly act on pro-inflammatory T cells in the aged brain (Fig. 7 F). To test this, we sort-purified CD4⁺ and CD8⁺ T cells from aged brains and cultured them in the presence or absence of IL-5. Anti-CD3, anti-CD28, IL-2, and IL-7 were added to the culture to ensure T cell survival. Notably, exposure to IL-5

abolished *Tnf* expression in purified CD8⁺ T cells within 24 h (Fig. 7 Q). The expression of *Tnf* by CD4⁺ cells was low and was not significantly altered by IL-5 (Fig. 7 Q). Exposure to IL-5 also reduced the expression of *Stat6b* and *Bnip3*, two IL-5 signaling targeted genes, in aged brain CD8⁺ T cells (Fig. 7 R). Consistent with elevated expression of *Bnip3*, CD8⁺ T cells cultured with IL-5 also exhibited increased apoptosis, demonstrated by increased percentage of Annexin V⁺ cells at day 3 of culture (Fig. 7 S). In contrast, culturing with IL-5 did not affect *Tnf* expression or the apoptotic rate of CD8⁺ T cells sorted from the spleens of aged mice (Fig. S5, B and C). Thus, IL-5 may specifically restrict the survival and TNF α expression of aging-associated brain-resident CD8⁺ T cells. Together, IL-5 may directly act on aging-associated pro-inflammatory T cells to restrain neuroinflammation, which may lead to enhanced neurogenesis and improved cognitive function.

Discussion

Our work has thus revealed the accumulation of tissue-resident ILC2 in the CP of aged brains and demonstrated that their activation may revitalize the aged brain and alleviate aging-associated cognitive decline. Interestingly, ILC2 in the aged brain are long-lived, capable of switching between cell cycle dormancy and proliferation, and resistant to cellular senescence and exhaustion under replication stress. When activated in vitro and transferred into the aged brain, they can drastically improve the cognitive function of aged mice. IL-5, a major effector molecule produced by ILC2, is sufficient to restrain aging-associated neuroinflammation and to alleviate aging-associated cognitive decline. Together, targeting these ILC2 in the aged brain may provide new avenues to combat brain aging.

Our data indicate that the effects of aging on immune cells are much more complicated than previously appreciated. Earlier work focused heavily on the detrimental effects of aging on the immune system. The term “immunosenescence” emerged to describe a decline in adaptive immunity and increased susceptibility to infectious diseases with aging (Goronzy and Weyand, 2013). Cellular senescence in immune cells was also linked with compromised functional capability, decreased self-renewal, and/or increased secretion of destructive pro-inflammatory cytokines (Coppé et al., 2010; Dilger and Johnson, 2008; Franceschi et al., 2018; Goronzy and Weyand, 2017). However, our study instead reveals that aging leads to the accumulation of a unique subset of brain ILC2 that exhibit enhanced cellular fitness, increased self-renewal, and robust beneficial functional capability. Despite their accumulation with age, ILC2 in the aged brain are resistant to cellular senescence and exhaustion in response to replication stress, which may lead to enhanced long-term self-renewal capability. ILC2 in the aged brain are functionally quiescent at homeostasis but can be vigorously activated and reactivated by exogenous stimuli. They possess potent functional capability to secrete beneficial effector molecules that restrain neuroinflammation and improve cognitive function. These results collectively suggest that aging may paradoxically select unique populations of lymphocytes with increased fitness, relative resistance to cellular senescence, and preserved

beneficial functional capability that may be harnessed to combat aging-associated diseases.

The brain is particularly susceptible to the effects of aging, with aging being the major risk factor for a variety of neurocognitive and neurodegenerative diseases. In this study, we have provided direct evidence that activated ILC2 can alleviate aging-associated cognitive decline. We have further defined a novel role for IL-5 in repressing aging-associated neuroinflammation and in improving the cognitive function of aged mice. Interestingly, we have not observed eosinophil growth in the aged brain after IL-5 treatment. Instead, IL-5 may directly repress the survival and production of pro-inflammatory cytokines of a unique subset of tissue-resident CD8⁺ T cells in the aged brain. Further efforts to generate aged eosinophil-deficient or aged CD8⁺ T cell-deficient mice would be worthwhile in understanding the intriguing roles of immune cells in brain aging. In addition, several anti-IL-5 and anti-IL5R α monoclonal antibodies have been Food and Drug Administration approved and are currently used to treat conditions such as asthma (Bleeker et al., 2016; Busse et al., 2019; Busse et al., 2018; Castro et al., 2018; Castro et al., 2015; Magnan et al., 2016; Ortega et al., 2014; Pavord et al., 2012). The potential effects of anti-IL-5 and anti-IL5R α treatments on memory and behavior may be worth future investigation.

Our results also revealed interesting differences in the transcriptomes and functional capability between meningeal and CP ILC2 in the aged brain. Compared with meningeal ILC2, CP ILC2 possess more potent capability to proliferate and to produce type 2 cytokines in response to IL-33. Both meningeal and CP ILC2 express high amounts of *Il1rl1* (encoding IL-33R) at comparable levels. Thus, other mechanisms likely contribute to their differential functional capability. Recent studies indicate that the developmental origins of ILC2 may influence their functional potential (Ricardo-Gonzalez et al., 2018; Schneider et al., 2019). In future efforts, it would be worthwhile to explore the ontogeny of meningeal and CP ILC2 in the context of aging, using aged lineage-tracing and other transgenic mice. Potential developmental origins of meningeal and CP ILC2 in aged mice include long-term self-renewal of fetal/postnatal precursor-derived cells, repopulation from adult bone marrow precursors, and repopulation from extramedullary precursors. It would be interesting to understand whether the distinctive property of ILC2 in the aged brain might be related to a unique developmental pathway. Of note, the CP is in close proximity to the HP and other brain parenchyma. Such a specialized anatomical location, together with their enhanced functional capability, suggests that CP ILC2 in the aged brain are a promising target for alleviating aging-associated cognitive decline.

Materials and methods

Mice

Young (2–3 mo) and aged (19–24 mo) female C57BL/6 mice were obtained from the National Institute of Aging via Charles River or bred in the animal facility of Albany Medical College. All animal experiments were performed according to protocols

approved by the Institutional Animal Care and Use Committee at Albany Medical College.

Human CP tissues

Deidentified human autopsy tissues were collected from deceased elderly people older than 65 yr. Specifically, CP tissues were dissected out freshly from ventricles of brains. Autopsy consents were obtained from family members. CP tissues were digested with 0.2 mg/ml of Liberase (Roche) and 0.1 mg/ml DNase I (Roche) in HBSS for 30 min at 37°C. Single-cell suspension was prepared followed by flow cytometry analysis. The Albany Medical College Institutional Review Board determined that this was not a human subject study because autopsy tissues were collected from deceased individuals.

Intravascular staining

Mice were injected i.v. with anti-CD45.2 PE (3 µg/mouse) and sacrificed 3 min later as described before (Anderson et al., 2014).

Isolation of hematopoietic cells

Mice were perfused with 50 ml of PBS into the right ventricle of the heart. The brain was harvested, minced, and digested with 0.2 mg/ml of Liberase (Roche) and 0.1 mg/ml DNase I (Roche) in HBSS for 30 min at 37°C. Single-cell suspension was made by filtering the tissue through a 70-µm strainer. Hematopoietic cells were harvested after gradient centrifugation with 40% Percoll (GE).

For isolation of hematopoietic cells from the meninges and CP, CP tissue lining the lateral ventricles was isolated. Leptomeninges attached to the brain parenchyma of the dorsal cerebrum were isolated and referred to as “Leptomeninges.” Meninges attached to the skull were isolated and referred to as “dura/arachnoid meninges.” CP and meninges were digested with 0.2 mg/ml of Liberase (Roche) and 0.1 mg/ml DNase I (Roche) in HBSS for 30 min at 37°C. Single-cell suspension was made by filtering the tissue through a 70-µm strainer.

Flow cytometry and cell sorting

Lineage markers include anti-B220 (RA3-6B2), anti-NK1.1 (PK136), anti-CD11b (M1/70), anti-CD3 (2C11), anti-CD5 (53-7.3), and anti-TCRβ (H57). Other antibodies include anti-CD45.2 (104), anti-Thy1.2 (53-2.1), anti-CD25 (PC61.5), anti-T1/ST2 (DJ8), anti-CD127 (A7R34), anti-Ki67 (16A8), anti-CD68 (FA11), anti-IL5 (TRFK5), anti-IL13 (ebio13A), and anti-GATA3 (TWAJ). Staining for transcription factors was performed using the Foxp3 Fix/Perm Kit (Thermo) according to the manufacturer's instructions, as we previously described (Shen et al., 2019; Shen et al., 2018; Yang et al., 2016; Yang et al., 2015; Yang et al., 2013; Yang et al., 2011; Zhang et al., 2017). Detection of EdU was performed using the Click-iT Plus EdU Flow Cytometry Assay Kit (Thermo) following the manufacturer's instructions. Detection of activated caspases was performed using the CaspGLOW staining kit (Thermo) according to the manufacturer's instructions. Intracellular cytokine staining was performed using the Cytofix/Cytoperm Kit (BD) following restimulation with PMA, ionomycin, and monensin at 37°C for 2.5 h, as we previously described (Shen et al., 2019; Shen et al., 2018; Yang et al.,

2016; Yang et al., 2015; Yang et al., 2013; Yang et al., 2011; Zhang et al., 2017). Flow cytometric analysis was performed using a FACSCanto analyzer (BD), and cell sorting was performed using a FACSaria II sorter (BD).

Cell culture and cytokine measurement

ILC2 were purified by fluorescence-activated cell sorting and cultured in α-MEM medium containing 20% Hyclone FCS (GE), SCF (100 ng/ml), IL-7 (20 ng/ml), IL-2 (20 ng/ml), and IL-33 (20 ng/ml). Cytokines were purchased from BioLegend. Cytokine concentrations were measured using the LEGENDplex Kit (BioLegend) following the manufacturer's instructions.

For T cell culture, CD4 or CD8 cells from the brains and spleens of aged mice were sorted and cultured in α-MEM medium containing 20% Hyclone FCS, anti-CD3 (1 µg/ml), anti-CD28 (2 µg/ml), IL-2 (20 ng/ml), and IL-7 (30 ng/ml). Round-bottom 96-well plates precoated with 10 µg/ml of anti-CD3 were used. 100 ng/ml of IL-5 was added to some wells. Antibodies were purchased from R&D. Cytokines were purchased from BioLegend.

Gene transcription analysis, microarray, and RNA-Seq

RNeasy Plus Mini Kit (Qiagen) was used to extract RNA from samples. qPCR was performed to examine gene expression. Microarray analysis was conducted at the Boston University Microarray and Sequencing Resource.

RNA-Seq was performed with the Center for Functional Genomics at the University at Albany. Samples for RNA-Seq were prepared from sorted cells into Trizol-LS, and cDNA was prepared using the SMART-Seq v4 Ultra Low Input RNA kit (Takara). Nextera XT DNA Library Prep Kit (Illumina) was used to generate the library, and NextSeq 500 (Illumina) was used to perform single-end, 75-bp, high-throughput sequencing. STAR aligner was used to align and normalize the data. DESeq2 was used for differential expression analysis. DAVID was used to perform gene pathway analysis (Huang et al., 2009a, 2009b). Heatmap was generated by Heatmapper (Babicki et al., 2016).

For scRNA-Seq, aged mice were treated with 400 ng of IL-33 daily for 7 d. Meningeal and CP ILC2 were sorted by fluorescence-activated cell sorting and pooled from 10 mice per group. scRNA-Seq was performed as we previously described (Harly et al., 2019). scRNA-Seq libraries were prepared using the chromium 5' single-cell gene expression kit (10× Genomics) according to the manufacturer's instruction. The library was sequenced by NextSeq 5000 (Illumina). Primary analysis was performed with Cellranger V3.1.0. Median numbers of unique molecular identifier counts were 4,225 for meningeal ILC2 and 5,347 for CP ILC2. Data were normalized and scaled using Seurat (Stuart et al., 2019). Cells were clustered by the UMAP function of Seurat using a dimension of 20. Violin plots were generated using Seurat normalized data. A Wilcoxon rank sum test was used to determine significance.

The microarray data of CP in young and aged mice have been deposited in the Gene Expression Omnibus under the accession no. GSE129923. The RNA-Seq data for cultured ILC2, microglia/T cells/ILC2 in IL-33-treated aged mice, and microglia/T cells in IL-5-treated aged mice have been deposited in Gene Expression

Omnibus under the accession nos. GSE129992, GSE129996, and GSE129999, respectively. scRNA-Seq data have been deposited in Gene Expression Omnibus under the accession no. GSE139328.

Cytokine injection, EdU labeling, and i.c.v. injection

For cytokine injections, mice were administrated with 2 μ g of IL-5 or 400 ng of IL-33 i.p. daily for 2 d or 7 d. For EdU labeling, mice were administrated i.p. with eight doses of EdU (100 mg/kg) over a 4-d course: one dose daily for the first 2 d, and three doses daily at 2-h interval for day 3 and day 4. For simultaneous administration of cytokine and EdU, EdU administration (100 mg/kg) started at day 1 of IL-5 treatment or day 3 of IL-33 treatment. Mice were euthanized, and EdU concentrations were examined by flow cytometry or immunofluorescence at 24 h or 4 wk after EdU labeling.

For i.c.v. injection, anesthetized mice were secured to the dorsal position on a stereotaxic device (Stoelting Co.) on a 37°C heat pad. 0.25% of bupivacaine (2 mg/kg; McGuff) was administered subcutaneously at the site of the incision. The site of injection was 0.4 mm posterior to the bregma and 1 ± 0.1 mm mediolateral. After the hair was removed, the skull at the injection spot was thinned using a microdrill and sterilely prepared PBS or cell suspension was loaded to a 10- μ l cone-tip microvolume syringe with a 26G needle (Trajan Scientific). The needle was lowered 2 mm into the brain using stereotaxic controls. The solutions were injected at a slow rate of 3 μ l over 3 min. Each mouse received injection of 10^5 ILC2, or 10 μ g of anti-IL-5 antibody (clone TRFK5; Bio X Cell) or isotype control, or sterile PBS control. The skin incision was sealed using surgical staples. Mice were rested for 1 wk before behavior tests.

CRISPR-mediated gene knockout

For CRISPR-mediated gene knockout, gRNAs were cloned into the lenti-CRISPRv2-GFP vector as we previously described (Shen et al., 2019). Lenti-CRISPRv2-GFP vector was a gift from David Feldser (University of Pennsylvania, Philadelphia, PA; Addgene plasmid #82416; Walter et al., 2017). The following gRNA sequences were used: 5'-ACGGAGGACGAGGCAGTTCC-3' (targeting *Il5*) and 5'-TGCGAATACGCCACGCGATGGG-3' (nontarget control). The gRNA sequences were previously published by Dr. Zheng Feng's laboratory (Sanjana et al., 2014). ILC2/b6 cell lines were expanded and activated in vitro with 10 ng/ml of IL-7, IL-2, and IL-33, as we described previously (Zhang et al., 2017). LC2/b6 line is an immortalized ILC2 cell line that exhibits the molecular and functional properties of activated ILC2 (Zhang et al., 2017). The transcriptome and functional capability of LC2/b6 cell lines were extensively characterized by our recent work (Hosokawa et al., 2019; Shen et al., 2019; Zhang et al., 2017). ILC2/b6 cells express all known ILC2 signature genes (Hosokawa et al., 2019; Shen et al., 2019; Zhang et al., 2017). They vigorously produce IL-5 and IL-13 in vitro and lack the production of IL-17, IL-22, IFN- γ , or other cytokines characteristic of the alternative lineage (Hosokawa et al., 2019; Shen et al., 2019; Zhang et al., 2017). Lentiviral transduction was performed with cultured ILC2/b6 cells, as we previously described (Hosokawa et al., 2019; Shen et al., 2019). GFP⁺ cells were sorted by fluorescence-activated cell sorting, and 10^5 cells were transferred into aged mice by i.c.v.

injection. The Object Placement Test was performed at 7 d after i.c.v. injection.

Behavior tests

Mice for behavior tests were group-housed with four mice per Allentown cage. Mice were habituated to the testing facility for 1 h before starting the behavior tests each day. The behavior tests were recorded and analyzed by using ANY-maze software (Stoelting Co.). Two independent experiments were performed for each behavior test.

The Object Placement Test was performed at 24 h after IL-5, IL-13, or IL-33 treatment or at 7 d after i.c.v. injection, as we previously described (Zuloaga et al., 2016). On day 1, mice explored in a 50 \times 50-cm white box for 10 min. On day 2, two identical objects were placed into the box with visual cues adhered to the walls of the box. Mice were allowed to explore for 20 min. On day 3, one of the objects was placed in a new location (the displaced object), and mice were allowed to explore for 20 min. Interaction was defined as sniffing and climbing within a 2-cm zone around the object. The percentage of time spent exploring the displaced object out of the total time interacting with both objects was calculated.

The Morris Water Maze test was performed at 4 d after IL-5 or IL-13 treatment or at 10 d after i.c.v. injection, as we previously described (Zuloaga et al., 2016). A circular pool with a diameter of 125 cm was used, with the water made opaque by nontoxic white paint and the temperature kept at 21°C–22°C. Visual cues were placed on four sides of the pool. The maze was conceptually divided into four quadrants. On day 1 (Visible trial), mice were trained to escape the maze by swimming to a clear plastic platform that was submerged by 1 cm in one of the four virtual quadrants (the target quadrant). The platform was made visible by black tape around the platform, with a 10-cm-tall black cylinder on top of it. Mice were trained for five trials of 3 min each. The mice were placed into the maze from two alternating locations opposite to the platform. A trial was concluded when the mouse found the platform and stayed on it for 10 s. If a mouse failed to escape the maze within 3 min, it was guided slowly to the platform by dragging its tail and stayed on the platform for 10 s. On day 2 (Hidden trial), mice were trained for five trials of 3 min each. The mice were made to escape the maze, but the visual cues on the platform were removed. A trial was concluded when the mouse found the platform and stayed on it for 10 s. If a mouse failed to escape the maze within 3 min, it was guided slowly to the platform by dragging its tail and stayed on the platform for 10 s. On day 3 (Probe trial), the platform was removed, and the mice were assessed by one test of 3 min. The percentage of time spent in the target quadrant out of the total test time during the Probe trial was calculated.

Immunofluorescence histology

For immunofluorescence staining of ILC2, whole-mount CP was fixed with 4% paraformaldehyde for 1 h at room temperature (RT), blocked with 10% normal rat serum in PBS for 1 h at RT, and stained with AF594 anti-CD3 (17A2; BioLegend) and AF647 anti-ICOS1 (C398.4; BioLegend) overnight at 4°C. CP was mounted onto slides with ProLong Antifade with DAPI solution

(Thermo). Slides were imaged using a Zeiss Axio Observer fluorescence microscope with a 10× objective. Images were processed by the Zeiss Zen Blue software.

Neurogenesis was examined as we previously described (Shen et al., 2008). Mice were treated with 2 µg of IL-5 and EdU (100 mg/kg) daily for 2 d followed by three doses of EdU (100 mg/kg) administration daily for another 2 d. Immunofluorescence histology was performed at 72 h after the last IL-5 injection (24 h after the last EdU administration). Mice were perfused with 50 ml of PBS followed by 50 ml of 4% paraformaldehyde. The brains were harvested and fixed for 24 h in 4% paraformaldehyde and transferred to 30% sucrose in PBS until the tissue sank. The brains were frozen in optimal cutting temperature compound and stored at −80°C until sectioning. The brains were sectioned at 40 µm using a Leica CM1950 cryostat and stained free-floating in a 24-well plate. To visualize EdU, the Click-iT Plus EdU Imaging Kit was used following the manufacturer's instructions. The sections were incubated with the blocking buffer consisting of 4% Normal Donkey Serum in PBS with 0.3% Triton X-100 for 1 h at RT and stained with anti-NeuN rabbit polyclonal ab (A60; Millipore) overnight at 4°C. Sections were then stained with Donkey anti-rabbit Rhodamine secondary antibody (Jackson) for 1 h at RT. Sections were mounted onto glass slides, and ProLong Gold Antifade solution (Invitrogen) was applied. Slides were imaged using the Axio Observer fluorescence microscope with a 10× objective. Images were processed by Zen Blue software, and EdU⁺ cells in the HP DG region were tallied blindly.

Statistical analysis

Wilcoxon rank sum test was used to determine significance in scRNA-Seq data. Two-tailed Student's *t* tests or ANOVA was used to calculate statistical significance in other experiments. *P* < 0.05 was considered significant.

Online supplemental material

Fig. S1 demonstrates the expression of representative genes by genome-wide microarray analysis of the bulk CP tissue from young and aged mice. Fig. S2 demonstrates the results of behavior tests in young or aged mice treated with PBS, IL-5, or IL-13. Fig. S3 shows tissue residency and gene expression of brain ILC2 in IL-33-treated aged mice. Fig. S4 shows the deletion efficiency of IL-5 in ILC2/b6 cells by CRISPR-mediated gene knockout technique. Fig. S5 shows that IL-5 did not promote the growth of brain eosinophils or the apoptosis of spleen CD8⁺ T cells from aged mice.

Acknowledgments

This work was supported by US National Institutes of Health grants R01HL137813, R01AG057782, and K22AI116728 (to Q. Yang) and R01NS110749 (to K.L. Zuloaga); the Alexandrine and Alexander L. Sinsheimer Scholar Award (to Q. Yang); and the American Heart Association Scientist Development Award 16SDG27190001 (to K.L. Zuloaga).

Author contributions: I.T.H. Fung, K.L. Zuloaga, and Q. Yang designed the study and wrote the manuscript. I.T.H. Fung

performed most of the experiments. P. Sankar, Y. Zhang, L.S. Robinson, X. Zhao, S.S. D'Souza, A.E. Salinero, Y. Wang, J. Qian, M.L. Kuentzel, S.V. Chittur, S. Temple, K.L. Zuloaga, and Q. Yang performed or helped perform some experiments. S. Temple helped design and interpret some experiments and edited the manuscript. All authors reviewed and approved the manuscript.

Disclosures: Dr. Yang reported a patent to US Provisional Application no. 62/822,159 (filed on March 22, 2019) pending. No other disclosures were reported.

Submitted: 22 May 2019

Revised: 28 October 2019

Accepted: 19 December 2019

References

- Anderson, K.G., K. Mayer-Barber, H. Sung, L. Beura, B.R. James, J.J. Taylor, L. Qunaj, T.S. Griffith, V. Vezys, D.L. Barber, and D. Masopust. 2014. Intravascular staining for discrimination of vascular and tissue leukocytes. *Nat. Protoc.* 9:209–222. <https://doi.org/10.1038/nprot.2014.005>
- Andersson, J., J. Cromvik, M. Ingelsten, C. Lingblom, K. Andersson, J.E. Johansson, and C. Wennerås. 2014. Eosinophils from hematopoietic stem cell recipients suppress allogeneic T cell proliferation. *Biol. Blood Marrow Transplant.* 20:1891–1898. <https://doi.org/10.1016/j.bbmt.2014.08.017>
- Arnold, I.C., M. Artola-Borán, P. Tallón de Lara, A. Kyburz, C. Taube, K. Ottemann, M. van den Broek, S. Yousefi, H.U. Simon, and A. Müller. 2018. Eosinophils suppress Th1 responses and restrict bacterially induced gastrointestinal inflammation. *J. Exp. Med.* 215:2055–2072. <https://doi.org/10.1084/jem.20172049>
- Babicki, S., D. Arndt, A. Marcu, Y. Liang, J.R. Grant, A. Maciejewski, and D.S. Wishart. 2016. Heatmapper: web-enabled heat mapping for all. *Nucleic Acids Res.* 44(W1):W147–53. <https://doi.org/10.1093/nar/gkw419>
- Bando, J.K., J.C. Nussbaum, H.E. Liang, and R.M. Locksley. 2013. Type 2 innate lymphoid cells constitutively express arginase-1 in the naive and inflamed lung. *J. Leukoc. Biol.* 94:877–884. <https://doi.org/10.1189/jlb.0213084>
- Baruch, K., N. Rosenzweig, A. Kertser, A. Deczkowska, A.M. Sharif, A. Spinrad, A. Tsitsou-Kampeli, A. Sarel, L. Cahalon, and M. Schwartz. 2015. Breaking immune tolerance by targeting Foxp3(+) regulatory T cells mitigates Alzheimer's disease pathology. *Nat. Commun.* 6:7967. <https://doi.org/10.1038/ncomms8967>
- Bleecker, E.R., J.M. FitzGerald, P. Chaney, A. Papi, S.F. Weinstein, P. Barker, S. Sproule, G. Gilmartin, M. Aurivillius, V. Werkström, and M. Goldman. SIROCCO study investigators. 2016. Efficacy and safety of benralizumab for patients with severe asthma uncontrolled with high-dosage inhaled corticosteroids and long-acting β_2 -agonists (SIROCCO): a randomised, multicentre, placebo-controlled phase 3 trial. *Lancet.* 388:2115–2127. [https://doi.org/10.1016/S0140-6736\(16\)31324-1](https://doi.org/10.1016/S0140-6736(16)31324-1)
- Brombacher, T.M., J.K. Nono, K.S. De Gouveia, N. Makena, M. Darby, J. Womersley, O. Tamgue, and F. Brombacher. 2017. IL-13-Mediated Regulation of Learning and Memory. *J. Immunol.* 198:2681–2688. <https://doi.org/10.4049/jimmunol.1601546>
- Busse, W.W., J.F. Maspero, K.F. Rabe, A. Papi, S.E. Wenzel, L.B. Ford, I.D. Pavord, B. Zhang, H. Staudinger, G. Pirozzi, et al. 2018. Liberty Asthma QUEST: Phase 3 Randomized, Double-Blind, Placebo-Controlled, Parallel-Group Study to Evaluate Dupilumab Efficacy/Safety in Patients with Uncontrolled, Moderate-to-Severe Asthma. *Adv. Ther.* 35:737–748. <https://doi.org/10.1007/s12325-018-0702-4>
- Busse, W., G. Chupp, H. Nagase, F.C. Albers, S. Doyle, Q. Shen, D.J. Bratton, and N.B. Gunsoy. 2019. Anti-IL-5 treatments in patients with severe asthma by blood eosinophil thresholds: Indirect treatment comparison. *J. Allergy Clin. Immunol.* 143:190–200.e20. <https://doi.org/10.1016/j.jaci.2018.08.031>
- Carson, M.J., J.M. Doose, B. Melchior, C.D. Schmid, and C.C. Ploix. 2006. CNS immune privilege: hiding in plain sight. *Immunol. Rev.* 213:48–65. <https://doi.org/10.1111/j.1600-065X.2006.00441.x>
- Castro, M., J. Zangrilli, M.E. Wechsler, E.D. Bateman, G.G. Brusselle, P. Bardini, K. Murphy, J.F. Maspero, C. O'Brien, and S. Korn. 2015. Reslizumab

- for inadequately controlled asthma with elevated blood eosinophil counts: results from two multicentre, parallel, double-blind, randomised, placebo-controlled, phase 3 trials. *Lancet Respir. Med.* 3:355–366. [https://doi.org/10.1016/S2213-2600\(15\)00042-9](https://doi.org/10.1016/S2213-2600(15)00042-9)
- Castro, M., J. Corren, I.D. Pavord, J. Maspero, S. Wenzel, K.F. Rabe, W.W. Busse, L. Ford, L. Sher, J.M. Fitzgerald, et al. 2018. Dupilumab Efficacy and Safety in Moderate-to-Severe Uncontrolled Asthma. *N. Engl. J. Med.* 378:2486–2496. <https://doi.org/10.1056/NEJMoal804092>
- Chen, Z., and B.D. Trapp. 2016. Microglia and neuroprotection. *J. Neurochem.* 136(Suppl 1):10–17. <https://doi.org/10.1111/jnc.13062>
- Coppé, J.P., P.Y. Desprez, A. Krtolica, and J. Campisi. 2010. The senescence-associated secretory phenotype: the dark side of tumor suppression. *Annu. Rev. Pathol.* 5:99–118. <https://doi.org/10.1146/annurev-pathol-121808-102144>
- Da Mesquita, S., A. Louveau, A. Vaccari, I. Smirnov, R.C. Cornelison, K.M. Kingsmore, C. Contarino, S. Onengut-Gumuscu, E. Farber, D. Raper, et al. 2018. Functional aspects of meningeal lymphatics in ageing and Alzheimer's disease. *Nature.* 560:185–191. <https://doi.org/10.1038/s41586-018-0368-8>
- Dansokho, C., D. Ait Ahmed, S. Aid, C. Toly-Ndour, T. Chaigneau, V. Calle, N. Cagnard, M. Holzenberger, E. Piaggio, P. Aucouturier, and G. Dorothée. 2016. Regulatory T cells delay disease progression in Alzheimer-like pathology. *Brain.* 139:1237–1251. <https://doi.org/10.1093/brain/awv408>
- Davis, S.M., and K.R. Pennypacker. 2018. The role of the leukemia inhibitory factor receptor in neuroprotective signaling. *Pharmacol. Ther.* 183: 50–57. <https://doi.org/10.1016/j.pharmthera.2017.08.008>
- de Rivero Vaccari, J.P., A. Marcillo, D. Nonner, W.D. Dietrich, and R.W. Keane. 2009. Neuroprotective effects of bone morphogenetic protein 7 (BMP7) treatment after spinal cord injury. *Neurosci. Lett.* 465:226–229. <https://doi.org/10.1016/j.neulet.2009.09.013>
- Derecki, N.C., A.N. Cardani, C.H. Yang, K.M. Quinnes, A. Cihfield, K.R. Lynch, and J. Kipnis. 2010. Regulation of learning and memory by meningeal immunity: a key role for IL-4. *J. Exp. Med.* 207:1067–1080. <https://doi.org/10.1084/jem.20091419>
- Di Paolo, N.C., S. Shafiani, T. Day, T. Papayannopoulou, D.W. Russell, Y. Iwakura, D. Sherman, K. Urdahl, and D.M. Shayakhmetov. 2015. Interdependence between Interleukin-1 and Tumor Necrosis Factor Regulates TNF-Dependent Control of Mycobacterium tuberculosis Infection. *Immunity.* 43:1125–1136. <https://doi.org/10.1016/j.immuni.2015.11.016>
- Dilger, R.N., and R.W. Johnson. 2008. Aging, microglial cell priming, and the discordant central inflammatory response to signals from the peripheral immune system. *J. Leukoc. Biol.* 84:932–939. <https://doi.org/10.1189/jlb.0208108>
- Faraco, G., D. Brea, L. Garcia-Bonilla, G. Wang, G. Racchumi, H. Chang, I. Buendia, M.M. Santisteban, S.G. Segarra, K. Koizumi, et al. 2018. Dietary salt promotes neurovascular and cognitive dysfunction through a gut-initiated TH17 response. *Nat. Neurosci.* 21:240–249. <https://doi.org/10.1038/s41593-017-0059-z>
- Finlay, C.M., A.M. Stefanska, K.P. Walsh, P.J. Kelly, L. Boon, E.C. Lavelle, P.T. Walsh, and K.H. Mills. 2016. Helminth Products Protect against Autoimmunity via Innate Type 2 Cytokines IL-5 and IL-33, Which Promote Eosinophilia. *J. Immunol.* 196:703–714. <https://doi.org/10.4049/jimmunol.1501820>
- Franceschi, C., P. Garagnani, P. Parini, C. Giuliani, and A. Santoro. 2018. Inflammaging: a new immune-metabolic viewpoint for age-related diseases. *Nat. Rev. Endocrinol.* 14:576–590. <https://doi.org/10.1038/s41574-018-0059-4>
- Fukushima, Y., N. Minato, and M. Hattori. 2018. The impact of senescence-associated T cells on immunosenescence and age-related disorders. *Inflamm. Regen.* 38:24. <https://doi.org/10.1186/s41232-018-0082-9>
- Gadani, S.P., I. Smirnov, A.T. Smith, C.C. Overall, and J. Kipnis. 2017. Characterization of meningeal type 2 innate lymphocytes and their response to CNS injury. *J. Exp. Med.* 214:285–296. <https://doi.org/10.1084/jem.20161982>
- Gasteiger, G., X. Fan, S. Dikiy, S.Y. Lee, and A.Y. Rudensky. 2015. Tissue residency of innate lymphoid cells in lymphoid and nonlymphoid organs. *Science.* 350:981–985. <https://doi.org/10.1126/science.aac9593>
- Glisky, E.L. 2007. Changes in cognitive function in human aging. In *Brain Aging: Models, Methods, and Mechanisms*. D.R. Riddle, editor. CRC Press, Boca Raton, FL. 3–20.
- Goronzy, J.J., and C.M. Weyand. 2013. Understanding immunosenescence to improve responses to vaccines. *Nat. Immunol.* 14:428–436. <https://doi.org/10.1038/ni.2588>
- Goronzy, J.J., and C.M. Weyand. 2017. Successful and Maladaptive T Cell Aging. *Immunity.* 46:364–378. <https://doi.org/10.1016/j.immuni.2017.03.010>
- Habbas, S., M. Santello, D. Becker, H. Stubbe, G. Zappia, N. Liaudet, F.R. Klaus, G. Kollias, A. Fontana, C.R. Pryce, et al. 2015. Neuroinflammatory TNF α Impairs Memory via Astrocyte Signaling. *Cell.* 163:1730–1741. <https://doi.org/10.1016/j.cell.2015.11.023>
- Hao, Y., P. O'Neill, M.S. Naradikian, J.L. Scholz, and M.P. Cancro. 2011. A B-cell subset uniquely responsive to innate stimuli accumulates in aged mice. *Blood.* 118:1294–1304. <https://doi.org/10.1182/blood-2011-01-330530>
- Harada, C.N., M.C. Natelson Love, and K.L. Triebel. 2013. Normal cognitive aging. *Clin. Geriatr. Med.* 29:737–752. <https://doi.org/10.1016/j.cger.2013.07.002>
- Harly, C., D. Kenney, G. Ren, B. Lai, T. Raabe, Q. Yang, M.C. Cam, H.H. Xue, K. Zhao, and A. Bhandardola. 2019. The transcription factor TCF-1 enforces commitment to the innate lymphoid cell lineage. *Nat. Immunol.* 20: 1150–1160. <https://doi.org/10.1038/s41590-019-0445-7>
- Hosokawa, H., M. Romero-Wolf, Q. Yang, Y. Motomura, D. Levanon, Y. Groner, K. Moro, T. Tanaka, and E.V. Rothenberg. 2019. Cell type-specific actions of Bcl11b in early T-lineage and group 2 innate lymphoid cells. *J. Exp. Med.* <https://doi.org/10.1084/jem.20190972>
- Huang, W., B.T. Sherman, and R.A. Lempicki. 2009a. Bioinformatics enrichment tools: paths toward the comprehensive functional analysis of large gene lists. *Nucleic Acids Res.* 37:1–13. <https://doi.org/10.1093/nar/gkn923>
- Huang, W., B.T. Sherman, and R.A. Lempicki. 2009b. Systematic and integrative analysis of large gene lists using DAVID bioinformatics resources. *Nat. Protoc.* 4:44–57. <https://doi.org/10.1038/nprot.2008.211>
- Ito, M., K. Komai, S. Mise-Omata, M. Iizuka-Koga, Y. Noguchi, T. Kondo, R. Sakai, K. Matsuo, T. Nakayama, O. Yoshie, et al. 2019. Brain regulatory T cells suppress astrogliosis and potentiate neurological recovery. *Nature.* 565:246–250. <https://doi.org/10.1038/s41586-018-0824-5>
- Kiyota, T., J. Machii, Y. Lu, B. Dyavarshetty, M. Nemati, I. Yokoyama, R.L. Mosley, and H.E. Gendelman. 2018. Granulocyte-macrophage colony-stimulating factor neuroprotective activities in Alzheimer's disease mice. *J. Neuroimmunol.* 319:80–92. <https://doi.org/10.1016/j.jneuroim.2018.03.009>
- Lingblom, C., J. Andersson, K. Andersson, and C. Wennerås. 2017. Regulatory Eosinophils Suppress T Cells Partly through Galectin-10. *J. Immunol.* 198:4672–4681. <https://doi.org/10.4049/jimmunol.1601005>
- Liu, Q., W. Xin, P. He, D. Turner, J. Yin, Y. Gan, F.D. Shi, and J. Wu. 2014. Interleukin-17 inhibits adult hippocampal neurogenesis. *Sci. Rep.* 4: 7554. <https://doi.org/10.1038/srep07554>
- López-Otin, C., M.A. Blasco, L. Partridge, M. Serrano, and G. Kroemer. 2013. The hallmarks of aging. *Cell.* 153:1194–1217. <https://doi.org/10.1016/j.cell.2013.05.039>
- Louveau, A., T.H. Harris, and J. Kipnis. 2015. Revisiting the Mechanisms of CNS Immune Privilege. *Trends Immunol.* 36:569–577. <https://doi.org/10.1016/j.it.2015.08.006>
- Magnan, A., A. Bourdin, C.M. Prazma, F.C. Albers, R.G. Price, S.W. Yancey, and H. Ortega. 2016. Treatment response with mepolizumab in severe eosinophilic asthma patients with previous omalizumab treatment. *Allergy.* 71:1335–1344. <https://doi.org/10.1111/all.12914>
- Marsh, S.E., E.M. Abud, A. Lakatos, A. Karimzadeh, S.T. Yeung, H. Davtyan, G.M. Fote, L. Lau, J.G. Weinger, T.E. Lane, et al. 2016. The adaptive immune system restrains Alzheimer's disease pathogenesis by modulating microglial function. *Proc. Natl. Acad. Sci. USA.* 113:E1316–E1325. <https://doi.org/10.1073/pnas.1525466113>
- McGowan, P.O., T.A. Hope, W.H. Meck, G. Kelsoe, and C.L. Williams. 2011. Impaired social recognition memory in recombination activating gene 1-deficient mice. *Brain Res.* 1383:187–195. <https://doi.org/10.1016/j.brainres.2011.02.054>
- Mesnil, C., S. Raulier, G. Paulissen, X. Xiao, M.A. Birrell, D. Pirottin, T. Janss, P. Starkl, E. Ramery, M. Henket, et al. 2016. Lung-resident eosinophils represent a distinct regulatory eosinophil subset. *J. Clin. Invest.* 126: 3279–3295. <https://doi.org/10.1172/JCI85664>
- Monticelli, L.A., M.D. Buck, A.L. Flamar, S.A. Saenz, E.D. Tait Wojno, N.A. Yudanin, L.C. Osborne, M.R. Hepworth, S.V. Tran, H.R. Rodewald, et al. 2016. Arginase 1 is an innate lymphoid-cell-intrinsic metabolic checkpoint controlling type 2 inflammation. *Nat. Immunol.* 17:656–665. <https://doi.org/10.1038/ni.3421>
- Nussbaum, J.C., S.J. Van Dyken, J. von Moltke, L.E. Cheng, A. Mohapatra, A.B. Molofsky, E.E. Thornton, M.F. Krummel, A. Chawla, H.E. Liang, and R.M. Locksley. 2013. Type 2 innate lymphoid cells control eosinophil homeostasis. *Nature.* 502:245–248. <https://doi.org/10.1038/nature12526>
- Ortega, H.G., M.C. Liu, I.D. Pavord, G.G. Brusselle, J.M. Fitzgerald, A. Chetta, M. Humbert, L.E. Katz, O.N. Keene, S.W. Yancey, and P. Chanez.

- MENSA Investigators. 2014. Mepolizumab treatment in patients with severe eosinophilic asthma. *N. Engl. J. Med.* 371:1198–1207. <https://doi.org/10.1056/NEJMoa1403290>
- Pan, W., C. Yu, H. Hsueh, R.S. Khan, and A.J. Kastin. 2009. Cerebral microvascular IL15 is a novel mediator of TNF action. *J. Neurochem.* 111: 819–827. <https://doi.org/10.1111/j.1471-4159.2009.06371.x>
- Pavord, I.D., S. Korn, P. Howarth, E.R. Bleeker, R. Buhl, O.N. Keene, H. Ortega, and P. Chané. 2012. Mepolizumab for severe eosinophilic asthma (DREAM): a multicentre, double-blind, placebo-controlled trial. *Lancet.* 380:651–659. [https://doi.org/10.1016/S0140-6736\(12\)60988-X](https://doi.org/10.1016/S0140-6736(12)60988-X)
- Ratcliff, M., S. Alter, D. Frasca, B.B. Blomberg, and R.L. Riley. 2013. In senescence, age-associated B cells secrete TNF α and inhibit survival of B-cell precursors. *Aging Cell.* 12:303–311. <https://doi.org/10.1111/ace.12055>
- Ricardo-Gonzalez, R.R., S.J. Van Dyken, C. Schneider, J. Lee, J.C. Nussbaum, H.E. Liang, D. Vaka, W.L. Eckalbar, A.B. Molofsky, D.J. Erle, and R.M. Locksley. 2018. Tissue signals imprint ILC2 identity with anticipatory function. *Nat. Immunol.* 19:1093–1099. <https://doi.org/10.1038/s41590-018-0201-4>
- Robinette, M.L., A. Fuchs, V.S. Cortez, J.S. Lee, Y. Wang, S.K. Durum, S. Gilfillan, and M. Colonna. Immunological Genome Consortium. 2015. Transcriptional programs define molecular characteristics of innate lymphoid cell classes and subsets. *Nat. Immunol.* 16:306–317. <https://doi.org/10.1038/ni.3094>
- Rubtsov, A.V., K. Rubtsova, A. Fischer, R.T. Meehan, J.Z. Gillis, J.W. Kappler, and P. Marrack. 2011. Toll-like receptor 7 (TLR7)-driven accumulation of a novel CD11c⁺ B-cell population is important for the development of autoimmunity. *Blood.* 118:1305–1315. <https://doi.org/10.1182/blood-2011-01-331462>
- Rubtsova, K., A.V. Rubtsov, M.P. Cancro, and P. Marrack. 2015. Age-Associated B Cells: A T-bet-Dependent Effector with Roles in Protective and Pathogenic Immunity. *J. Immunol.* 195:1933–1937. <https://doi.org/10.4049/jimmunol.1501209>
- Sanjana, N.E., O. Shalem, and F. Zhang. 2014. Improved vectors and genome-wide libraries for CRISPR screening. *Nat. Methods.* 11:783–784. <https://doi.org/10.1038/nmeth.3047>
- Schneider, C., J. Lee, S. Koga, R.R. Ricardo-Gonzalez, J.C. Nussbaum, L.K. Smith, S.A. Villeda, H.E. Liang, and R.M. Locksley. 2019. Tissue-Resident Group 2 Innate Lymphoid Cells Differentiate by Layered Ontogeny and In Situ Perinatal Priming. *Immunity.* 50:1425–1438.e5. <https://doi.org/10.1016/j.immuni.2019.04.019>
- Shen, Q., Y. Wang, E. Kokovay, G. Lin, S.M. Chuang, S.K. Goderie, B. Roysam, and S. Temple. 2008. Adult SVZ stem cells lie in a vascular niche: a quantitative analysis of niche cell-cell interactions. *Cell Stem Cell.* 3: 289–300. <https://doi.org/10.1016/j.stem.2008.07.026>
- Shen, X., M.A. Pasha, K. Hidde, A. Khan, M. Liang, W. Guan, Y. Ding, A. Haczk, and Q. Yang. 2018. Group 2 innate lymphoid cells promote airway hyperresponsiveness through production of VEGFA. *J. Allergy Clin. Immunol.* 141:1929–1931.e4. <https://doi.org/10.1016/j.jaci.2018.01.005>
- Shen, X., M. Liang, X. Chen, M.A. Pasha, S.S. D'Souza, K. Hidde, J. Howard, D.A. Sultana, I.T.H. Fung, L. Ye, et al. 2019. Cutting Edge: Core Binding Factor β Is Required for Group 2 Innate Lymphoid Cell Activation. *J. Immunol.* 202:1669–1673. <https://doi.org/10.4049/jimmunol.1800852>
- Spittau, B. 2017. Aging Microglia-Phenotypes, Functions and Implications for Age-Related Neurodegenerative Diseases. *Front. Aging Neurosci.* 9:194. <https://doi.org/10.3389/fnagi.2017.00194>
- Stuart, T., A. Butler, P. Hoffman, C. Hafemeister, E. Papalexi, W.M. Mauck III, Y. Hao, M. Stoeckius, P. Smibert, and R. Satija. 2019. Comprehensive Integration of Single-Cell Data. *Cell.* 177:1888–1902.e21. <https://doi.org/10.1016/j.cell.2019.05.031>
- Terrando, N., C. Monaco, D. Ma, B.M. Foxwell, M. Feldmann, and M. Maze. 2010. Tumor necrosis factor- α triggers a cytokine cascade yielding postoperative cognitive decline. *Proc. Natl. Acad. Sci. USA.* 107: 20518–20522. <https://doi.org/10.1073/pnas.1014557107>
- Vivier, E., D. Artis, M. Colonna, A. Diefenbach, J.P. Di Santo, G. Eberl, S. Koyasu, R.M. Locksley, A.N.J. McKenzie, R.E. Mebius, et al. 2018. Innate Lymphoid Cells: 10 Years On. *Cell.* 174:1054–1066. <https://doi.org/10.1016/j.cell.2018.07.017>
- Walter, D.M., O.S. Venancio, E.L. Buza, J.W. Tobias, C. Deshpande, A.A. Gu-diel, C. Kim-Kiselak, M. Cicchini, T.J. Yates, and D.M. Feldser. 2017. Systematic In Vivo Inactivation of Chromatin-Regulating Enzymes Identifies Setd2 as a Potent Tumor Suppressor in Lung Adenocarcinoma. *Cancer Res.* 77:1719–1729. <https://doi.org/10.1158/0008-5472.CAN-16-2159>
- Wilson, A., E. Laurenti, G. Oser, R.C. van der Wath, W. Blanco-Bose, M. Jaworski, S. Offner, C.F. Dunant, L. Eshkind, E. Bockamp, et al. 2008. Hematopoietic stem cells reversibly switch from dormancy to self-renewal during homeostasis and repair. *Cell.* 135:1118–1129. <https://doi.org/10.1016/j.cell.2008.10.048>
- Wolf, S.A., B. Steiner, A. Akpınarlı, T. Kammertoens, C. Nassenstein, A. Braun, T. Blankenstein, and G. Kempermann. 2009. CD4-positive T lymphocytes provide a neuroimmunological link in the control of adult hippocampal neurogenesis. *J. Immunol.* 182:3979–3984. <https://doi.org/10.4049/jimmunol.0801218>
- Yang, Q., and A. Bhandoola. 2016. The development of adult innate lymphoid cells. *Curr. Opin. Immunol.* 39:114–120. <https://doi.org/10.1016/j.coi.2016.01.006>
- Yang, Q., S.A. Saenz, D.A. Zlotoff, D. Artis, and A. Bhandoola. 2011. Cutting edge: Natural helper cells derive from lymphoid progenitors. *J. Immunol.* 187:5505–5509. <https://doi.org/10.4049/jimmunol.1102039>
- Yang, Q., L.A. Monticelli, S.A. Saenz, A.W. Chi, G.F. Sonnenberg, J. Tang, M.E. De Obaldia, W. Bailis, J.L. Bryson, K. Toscano, et al. 2013. T cell factor 1 is required for group 2 innate lymphoid cell generation. *Immunity.* 38: 694–704. <https://doi.org/10.1016/j.immuni.2012.12.003>
- Yang, Q., F. Li, C. Harly, S. Xing, L. Ye, X. Xia, H. Wang, X. Wang, S. Yu, X. Zhou, et al. 2015. TCF-1 upregulation identifies early innate lymphoid progenitors in the bone marrow. *Nat. Immunol.* 16:1044–1050. <https://doi.org/10.1038/ni.3248>
- Yang, Q., M.Q. Ge, B. Kokalari, I.G. Redai, X. Wang, D.M. Kemeny, A. Bhandoola, and A. Haczk. 2016. Group 2 innate lymphoid cells mediate ozone-induced airway inflammation and hyperresponsiveness in mice. *J. Allergy Clin. Immunol.* 137:571–578. <https://doi.org/10.1016/j.jaci.2015.06.037>
- Yarilina, A., K.H. Park-Min, T. Antoniv, X. Hu, and L.B. Ivashkiv. 2008. TNF activates an IRF1-dependent autocrine loop leading to sustained expression of chemokines and STAT1-dependent type I interferon-response genes. *Nat. Immunol.* 9:378–387. <https://doi.org/10.1038/ni1576>
- Zhang, K., X. Xu, M.A. Pasha, C.W. Siebel, A. Costello, A. Haczk, K. Mac-Namara, T. Liang, J. Zhu, A. Bhandoola, et al. 2017. Cutting Edge: Notch Signaling Promotes the Plasticity of Group-2 Innate Lymphoid Cells. *J. Immunol.* 198:1798–1803. <https://doi.org/10.4049/jimmunol.1601421>
- Zuloaga, K.L., L.A. Johnson, N.E. Roesse, T. Marzulla, W. Zhang, X. Nie, F.N. Alkayed, C. Hong, M.R. Grafe, M.M. Pike, et al. 2016. High fat diet-induced diabetes in mice exacerbates cognitive deficit due to chronic hypoperfusion. *J. Cereb. Blood Flow Metab.* 36:1257–1270. <https://doi.org/10.1177/0271678X15616400>

Supplemental material

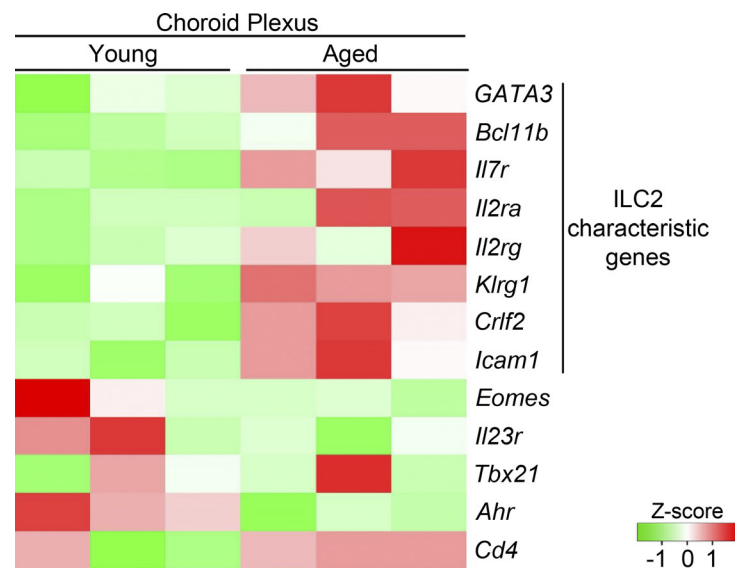


Figure S1. **The expression of many ILC2 characteristic genes is upregulated in the CP of aged mice.** Heatmap depicts the expression of the indicated genes in the CP of young and aged mice by genome-wide microarray analysis.

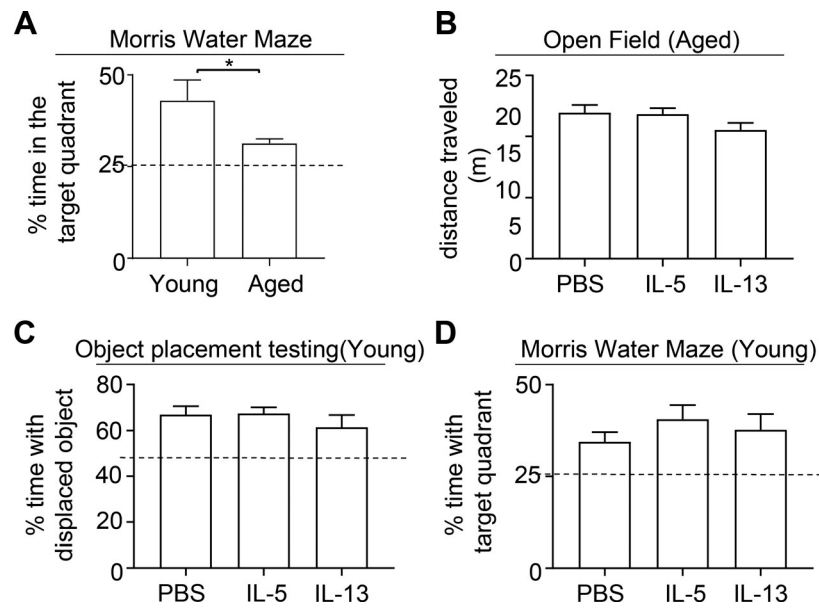


Figure S2. **Behavior test results in young and aged mice treated with PBS, IL-5, or IL-13.** (A) The Morris Water Maze test was performed with young or aged mice. Percentage of time spent in the target quadrant was quantified. Data are from six to eight mice per group and are representative of two independent experiments. (B) Distance traveled in the Open Field Test for aged mice treated with PBS, IL-5, or IL-13. Data are from 9 or 10 mice per group and are representative of two independent experiments. (C) The Object Placement Test was performed with young mice treated with PBS, IL-5, or IL-13. Percentage of time with the displaced object was quantified. Data are from eight mice per group and are representative of two independent experiments. (D) The Morris Water Maze test was performed with young mice treated with PBS, IL-5, or IL-13. Percentage of time spent in the target quadrant was quantified. Data are from 11–15 mice per group, pooled from two independent experiments. Error bars are mean \pm SEM. *, $P < 0.05$.

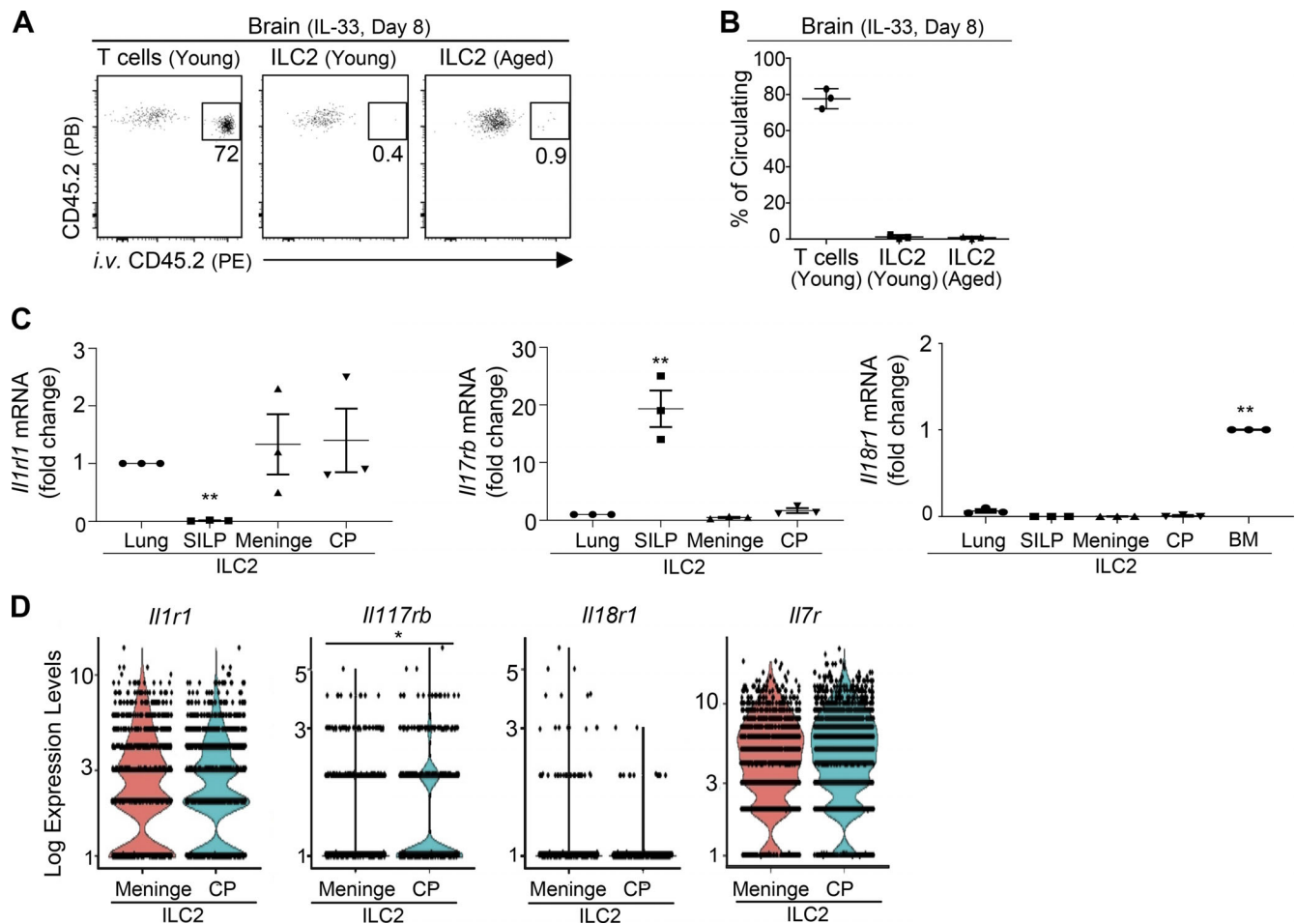


Figure S3. **Tissue residency and gene expression of brain ILC2 in IL-33-treated aged mice.** (A) Young or aged mice were treated with IL-33 daily for 7 d. At 24 h after the last injection, mice were injected with anti-CD45.2 PE antibody i.v. and euthanized 3 min later. Flow cytometry was performed to examine circulating cells that were labeled with i.v. injected anti-CD45.2 PE antibody. Representative flow cytometry profiles. Plots were pregated on brain T cells or ILC2. (B) Percentages of circulating cells in IL-33-treated mice. Data are from three mice per group and are representative of two independent experiments. (C) qPCR analysis of the indicated genes in ILC2 sorted from different anatomical sites at homeostasis. Data are from three mice per group, pooled from three independent experiments. SILP, small intestinal lamina propria; BM, bone marrow. (D) Expression of the indicated genes in CP and meninges of ILC2 in IL-33-treated mice by scRNA-Seq. Error bars are mean \pm SEM. *, $P < 0.05$; **, $P < 0.01$.

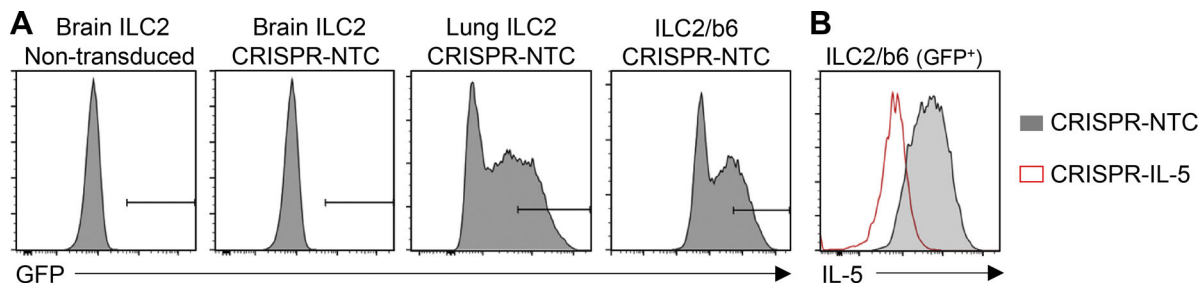


Figure S4. **Efficient deletion of IL-5 in ILC2/b6 cells.** (A) Brain ILC2 from aged mice were transduced with lenti-CRISPRv2-GFP lentivirus containing an NTC sequence. GFP expression was examined at 5 d after transduction. Cells without lentiviral transduction, lung ILC2 sorted from young mice, and an immortalized ILC2 line ILC2/b6 were used as controls. Data represent four independent experiments. (B) ILC2/b6 line cells were transduced with lenti-CRISPRv2-GFP lentivirus containing a gRNA targeting IL-5 or NTC. Expression of IL-5 was examined at 10 d after transduction. Data represent three independent experiments.

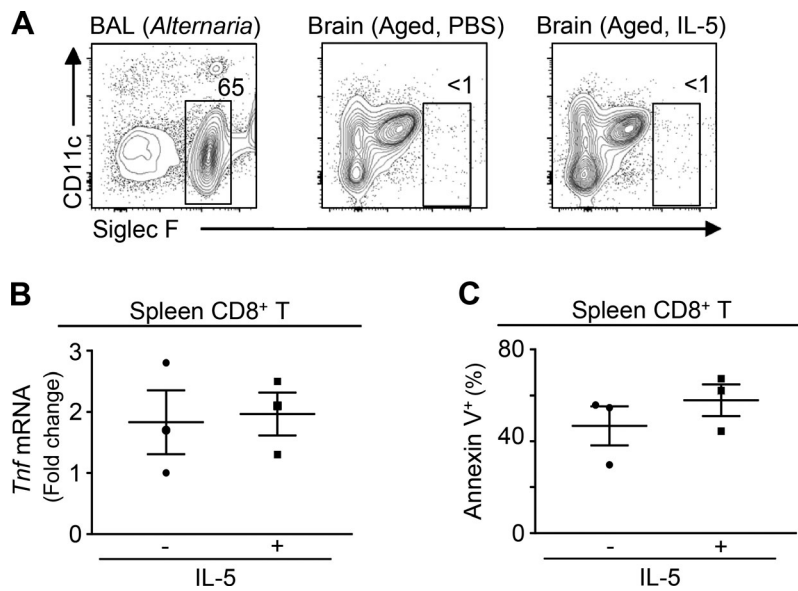


Figure S5. IL-5 did not induce proliferation of brain eosinophils or the apoptosis of spleen CD8⁺ T cells in aged mice. (A) Aged mice were treated with IL-5 daily for 2 d. Brains were harvested, and immune cells were examined by flow cytometry analysis at 24 h after last injection. Bronchoalveolar lavage (BAL) cells from young mice that inhaled 40 μ g of *Alternaria alternata* extract daily for 3 d were used as positive controls for eosinophil staining. Data are from three mice per group and are representative of two independent experiments. (B) Spleen CD8⁺ T cells were sorted from aged mice and cultured with anti-CD3, anti-CD8, IL-7, and IL-2 in the presence or absence of IL-5. mRNA of *Tnf* was examined at 24 h of culture. (C) Annexin V staining was performed with aged spleen CD8⁺ T cells after 3 d of culture. Data are from three mice per group and are representative of two independent experiments. Error bars are mean \pm SEM.